Marián Palcut

Cation diffusion in $LaMnO_3$, $LaCoO_3$ and $LaFeO_3$ materials

Thesis for the degree of philosophiae doctor

Trondheim, June 2007

Norwegian University of
Science and Technology
Faculty of Natural Sciences and Technology
Department of Materials Science and Engineering

NTNU
Innovation and Creativity

NTNU
Norwegian University of Science and Technology

Thesis for the degree of philosophiae doctor

Faculty of Natural Sciences and Technology
Department of Materials Science and Engineering

ISBN 978-82-471-3795-6 (printed ver.)
ISBN 978-82-471-3800-7 (electronic ver.)
ISSN 1503-8181
IMT-report: 2007:93
IUK-Thesis 123

Theses at NTNU, 2007:173

Printed by Tapir Uttrykk

This thesis has been submitted to

Department of Materials Science and Engineering
Norwegian University of Science and Technology

in partial fulfilment of the requirements for
the academic degree

Philosophiae doctor

June 2007

Preface

The work this thesis is based on was carried out at the Department of Materials Science and Engineering (previously known as the Department of Materials Technology) of the Norwegian University of Science and Technology in Trondheim, Norway during the period August 2004 – June 2007. I worked under the joint supervision of Prof. Tor Grande and Assoc. Prof. Kjell Wiik. The financial support was provided by the Research Council of Norway, grant no. 158517/431, Functional oxides for energy technology. Parts of this thesis were published or are under the consideration for publication in the following journals and conference proceedings:

1. Palcut, M.; Wiik, K.; Grande, T.: Determination of Mn^{3+} diffusion in $LaMnO_3$ based on solid state reaction method. Solid State Electrochemistry, Proceedings of the 26th Risø International Symposium on Materials Science, Roskilde, Denmark, Sept. 4-8, 2005 (2005), 297-303. ISBN 87-550-3455-1, ISSN 0970-0079.
2. Palcut, M.; Wiik, K.; Grande, T.: Cation diffusion in $LaCoO_3$. Inorganic Membranes, Proceedings of the 9th International Conference on Inorganic Membranes, Lillehammer, Norway, June 25-29, 2006 (2006), ISBN 82-14-04026-5.
3. Palcut, M.; Wiik, K.; Grande, T.: Cation self-diffusion and nonstoichiometry of lanthanum manganite studied by diffusion couple measurements. Journal of Physical Chemistry C (2007), 111(2), 813-822.
4. Palcut, M.; Wiik, K.; Grande, T.: Cation self-diffusion in $LaCoO_3$ and La_2CoO_4 studied by diffusion couple experiments. Journal of Physical Chemistry B (2007), 111(9), 2299-2308.
5. Palcut, M.; Wiik, K.; Christensen, J. S.; Grande, T.: Tracer diffusion of ^{141}Pr in $LaMnO_3$, $LaCoO_3$ and $LaFeO_3$ materials. Journal of Physical Chemistry, submitted on 7th May 2007.
6. Palcut, M.; Wiik, K.; Grande, T.: Cation inter-diffusion between $LaMnO_3$ and $LaCoO_3$ materials. Journal of Physics and Chemistry of Solids, submitted on 16th June 2007.

I would like to express my gratitude to my advisors, Prof. Tor Grande and Assoc. Prof. Kjell Wiik, for giving me the opportunity to work on this project for my PhD. They were always encouraging and supportive. Many thanks go also to Prof. Signe Kjelstrup and Prof. Dick Bedeaux from the Department of Chemistry for their interest in my work.

Experimental part of this work wouldn't be possible without the occasional help from technicians and fellow master and doctoral students and postdocs at the department – thank you all! My thanks go to my office-mates, Espen André Rudberg and Morten Jensen Sundheim, and to the rest of ceramic group. My special gratitude goes to Ms. Eli Beate Jakobsen who helped me to build a high temperature furnace that has been functioning perfectly in the last three years.

Finally, I would like to thank my parents and my sister and new and old friends for being there for me when I needed their helping hand. Especially the Czecho-Slovak group of friends in Trondheim must be acknowledged: Michal Tkáč, Jana Hajasová,

Martin Keppert, Silvie Švarcová, Eva Bartoníčková, Roman Kodým, Svatopluk Chytil, Pavel Petrovič, Michal Galík and Magdaléna Ovečková.

Trondheim, June 2007 Marián Palcut

Table of contents

1. Summary

Long term materials stability is one of the main challenges related to the development of electrochemical devices such as solid oxide fuel cells (SOFC) and dense gas separation membranes. These devices often operate under severe conditions. Gradients in thermodynamic potentials may lead over time to the transport of species which are initially expected to have a very low mobility. The reduction of the performance of fuel cells is related to the deterioration of materials properties due to interfacial reactions and inter-diffusion between the different fuel cell components. Degradation mechanisms of oxygen permeable membranes exposed to a gradient in the chemical potential of oxygen include cation demixing and decomposition. The development of SOFC and dense inorganic membranes technology must, therefore, take into consideration a possible transport of cations. Here a study of cation diffusion in $LaMnO_3$, $LaCoO_3$ and $LaFeO_3$ materials is presented. Substituted derivatives of these materials are key components in SOFC electrodes and oxygen permeable membranes. A set of experiments including reactive diffusion couples, inter-diffusion measurements and tracer diffusion experiments has been performed in order to evaluate the diffusion coefficients and contribute further to general understanding of defect chemistry and transport properties of perovskites. The results are presented in four separate papers and an overview of the experiments is given the following table:

Material	Cation	T / K	p_{O_2} / kPa	Reference
$LaMnO_3$	Mn^{3+}	1370 – 1673	0.04 – 50	Paper I
$LaCoO_3$	Co^{3+}	1370 – 1673	0.04 - 50	Paper II
La_2CoO_4	Co^{3+}	1573	0.04	Paper II
$LaMnO_3$	Pr^{3+}	1373 - 1673	21	Paper III
$LaCoO_3$	Pr^{3+}	1373 - 1673	21	Paper III
$LaFeO_3$	Pr^{3+}	1373 - 1673	21	Paper III
$LaMn_{1-x}Co_xO_3$(ss)	Co^{3+}	1383 - 1683	21	Paper IV

In paper I, reaction kinetics between dense, polycrystalline pellets of La_2O_3 and Mn_3O_4 was investigated at temperatures 1370-1673 K and oxygen partial pressures 40 Pa - 50 kPa. The formation of a single product phase, nonstoichiometric $La_{1-x}Mn_{1-y}O_{3\pm\delta}$, was confirmed by X-ray diffraction and electron microprobe analysis. The solid solubility limits of $La_{1-x}Mn_{1-y}O_{3\pm\delta}$ determined by wave dispersive spectroscopy were in good agreement with previous reports and equilibrium was achieved at the phase boundaries in the diffusion couples. The growth of the product phase followed the parabolic rate law regardless of temperature and oxygen partial pressure. The location of Pt-markers demonstrated that the diffusion of Mn cations in $La_{1-x}Mn_{1-y}O_{3\pm\delta}$ dominated over the diffusion of La^{3+}. The diffusion coefficient of Mn^{3+} was determined from the parabolic rate constant and activation energy of (280±40) kJ mol^{-1} was found. The analysis of the observed solubility limits of the $LaMnO_3$ phase suggested that a considerable amount of Mn vacancies was present only in a thin layer close to the $LaMnO_3/La_2O_3$ interface at low temperatures and

high oxygen partial pressures. The vacancies at the La and O sub-lattices were proposed to be the dominating point defects in the product layer. The chemical diffusion coefficient of Mn cations increased with decreasing pO_2 and increasing temperature. At low pO_2, the entire $LaMnO_3$ phase was La-deficient. It is therefore likely that the Mn vacancy diffusion took place also in the La sublattice. The results were discussed in relation to cation diffusion in other $LaBO_{3\pm\delta}$ oxides (B = Cr^{3+}, Mn^{3+}, Fe^{3+}).

In paper II, reaction kinetics between dense, polycrystalline pellets of La_2O_3 and CoO were investigated at temperatures 1370-1673 K and oxygen partial pressures 40 Pa - 50 kPa. At high oxygen partial pressures, single phase $LaCoO_3$ was formed. The growth of the $LaCoO_3$ phase followed the parabolic rate law. The location of Pt-markers demonstrated that the diffusion of Co cations in $LaCoO_3$ dominated over the diffusion of La^{3+}. The diffusion coefficient of Co^{3+} was determined from the parabolic rate constant and an activation energy of (250±10) kJ mol^{-1} was found. The diffusion coefficient of Co^{3+} in $LaCoO_3$ decreased with decreasing oxygen partial pressure. The defect chemistry of $LaCoO_3$ is dominated by oxygen vacancies. Due to the Schottky defect equilibria taking place in the material the concentration of cobalt vacancies increases with the pO_2. The diffusion coefficient of Co^{3+} cations followed the increase in the concentration of cobalt vacancies which reflects the vacancy mechanism of the chemical diffusion. The results obtained for the $LaCoO_3$ phase were discussed in relation to cation diffusion in other $LnBO_3$ oxides (B = Cr^{3+}, Mn^{3+}, Fe^{3+}). A correlation between the diffusivity of the B-cation and the melting point was found for the $LnBO_3$ materials. The relationship between the chemical diffusion coefficient and the melting point suggests that the melting process of the crystal lattice of perovskites is related to the stability of the BO_6 network rather than to the mobility of the A cation. At the lowest oxygen partial pressure investigated, two product phases in the diffusion couples La_2O_3 - CoO were observed - $LaCoO_3$ and La_2CoO_4. La_2CoO_4 is a Ruddelsden-Popper phase, which contains the perovskite layers altered with the LaO rock salt layers. The analysis of the data revealed that the diffusion of Co cations in La_2CoO_4 and $LaCoO_3$ phases was comparable despite of the layered structure of the La_2CoO_4 phase. It can, therefore, be suggested that the diffusion of Co cations in the La_2CoO_4 phase takes place both in the perovskite layer and along the *c*-axis – probably via vacant La sites in the LaO layer.

In paper III, impurity diffusion of Pr^{3+} in dense polycrystalline $LaMnO_3$, $LaCoO_3$ and $LaFeO_3$ respectively was studied at 1373 – 1673 K in air in order to shed a light on the La-site vacancy migration in these materials. Cation distribution profiles were studied by secondary ion mass spectrometry and it was found that penetration profiles of Pr^{3+} had two distinct regions with different slopes. The first, shallow region was used to evaluate the bulk diffusion coefficients. The activation energies for bulk diffusion of Pr^{3+} in $LaMnO_3$, $LaCoO_3$ and $LaFeO_3$ were (47 ± 31), (141 ± 40) and (198 ± 84) kJ mol^{-1} respectively, which are significantly lower than previously predicted by atomistic simulations. The bulk diffusion coefficients of Pr^{3+} cations in $LaCoO_3$ and $LaFeO_3$ materials were about 1-2 orders of magnitude lower than the chemical self-diffusion coefficients of the Co^{3+} and Fe^{3+} cations respectively. The bulk diffusion of Pr^{3+} in $LaMnO_3$ was enhanced compared to $LaCoO_3$ and $LaFeO_3$ materials due to higher concentrations of intrinsic point defects in $LaMnO_3$, especially La-site vacancies. The grain boundary diffusion coefficients of Pr^{3+} in

$LaCoO_3$ and $LaFeO_3$ materials were evaluated according to the Whipple-Le Claire's equation. Activation energies for grain boundary diffusion of Pr^{3+} in $LaCoO_3$ and $LaFeO_3$ materials respectively were (173 ± 24) and (196 ± 74) kJ mol^{-1} respectively. A correlation between activation energies for cation diffusion in bulk and along grain boundaries in pure and substituted $LaBO_3$ materials (B = Cr, Fe, Co) was found and discussed. It may be suggested that the cation diffusion is of the vacancy type both inside the grains and along grain boundaries. The grain boundary diffusion, however, is accelerated due to the significant amount of defects located at grain boundaries.

In paper IV, cation inter-diffusion between $LaMnO_3$ and $LaCoO_3$ materials was investigated at 1383 – 1683 K in air by electron microprobe analysis. The penetration of Co^{3+} into $LaMnO_3$ was observed to be significantly more pronounced than the Mn^{3+} diffusion in $LaCoO_3$. The inter-diffusion of Co^{3+} into $LaMnO_3$ resulted in the formation of solid solution $LaMn_{1-x}Co_xO_3$(ss) in line with previous phase diagram studies. The bulk diffusion coefficients of Co^{3+} in $LaMn_{1-x}Co_xO_3$(ss) were evaluated and an activation energy of (197 ± 17) kJ mol^{-1} was found. The element mapping of the exposed surface of $LaCoO_3$ revealed a preferential grain boundary diffusion of Mn^{3+} in $LaCoO_3$. The low bulk diffusion of Mn^{3+} in $LaCoO_3$ relative to bulk diffusion of Co^{3+} in $LaMnO_3$ reflects the lower cation vacancy concentration in the later material. The difference in the activation energies for the impurity diffusion of Co^{3+} in $LaMnO_3$ and self-diffusion of Mn^{3+} in $LaMnO_3$ reported previously, was discussed with respect to the contributions of vacancy formation and migration enthalpies reflecting the different thermal history of the materials. The estimated apparent enthalpies for the partial Schottky equilibrium of $LaMnO_3$ and $LaCoO_3$ materials were similar but significantly lower than previously calculated by atomistic simulations.

The diffusion of the B cation (B = Mn, Fe, Co) in $LaMnO_3$, $LaFeO_3$ and $LaCoO_3$ materials respectively was found to be dominating over the La^{3+} diffusion. This observation is unexpected from structural considerations of the perovskite phase since two neighbouring B^{3+} lattice positions are separated by an oxygen anion, while two La^{3+} lattice positions are not. The activation barrier for the simple vacancy hopping in the B cation sublattice was initially expected to be high. Nevertheless, the experiments confirmed that the activation energies for the Mn^{3+}, Fe^{3+} and Co^{3+} diffusion in $LaMnO_3$, $LaFeO_3$ and $LaCoO_3$ materials were considerably lower. We therefore suggested that the B cation diffusion in $LaMnO_3$, $LaFeO_3$ and $LaCoO_3$ materials did not take place solely in the B sublattice. A possible migration mechanism discussed in this thesis was the diffusion of the B cations via both the La and B vacant sites. This mechanism provides a substantial decrease of the activation barrier. The amount of available cation vacancies in the materials is a critical point with this respect. Although the $LaMnO_3$ phase is known to exhibit a significant cation deficiency and has a significant amount of vacancies, the $LaCoO_3$ and $LaFeO_3$ phases are nearly cation stoichiometric and thus, possess only a small amount of cation vacancies. The diffusivities and activation energies for the B cation self-diffusion in $LaMnO_3$, $LaFeO_3$ and $LaCoO_3$ materials were similar. This fact indicates that the B cation diffusion occurred by the same mechanism in all three materials despite of the different defect chemistry of the materials involved. It is, therefore, believed that the number of cation vacancies required to facilitate the B cation diffusion was relatively low and it was

provided by a common defect reaction taking place in each of the three materials. The source of cation vacancies could be either a full Schottky equilibrium or a partial Schottky defect equilibrium occurring at one of the interfaces in reactive diffusion couples.

2. Background

Materials based on perovskite-type $LaMnO_3$, $LaCoO_3$ and $LaFeO_3$ are often used as the components of high temperature devices. These include solid oxide fuel cells[1,2] and oxygen permeable membranes.[3,4,5] The component materials operate under various thermodynamic forces. The exposure to thermodynamic gradients of temperature, pressure or electrical field leads to transport processes of mobile components and causes the materials degradation and decrease of performance.

If an oxide with a composition $(A_{1-x}B_x)O$ is exposed to an oxygen potential gradient, the gradients of the chemical potentials of the chemical components A and B are induced as a consequence of the Gibbs-Duhem relation, $x_A d\mu_A + x_B d\mu_B + x_O d\mu_O = 0$.[6] This situation is illustrated in Fig. 2.1.[6] The thermodynamic forces generate fluxes of the mobile components. The cations are assumed to be mobile by the means of cation vacancies, V, in the cation sublattice of the binary oxide. The fluxes of cations and vacancies are, therefore, coupled. If both cations have different mobilities, the originally homogeneous oxide becomes inhomogeneous (Fig. 2.1b).[6] The faster of the two cations becomes enriched at the high-$p(O_2)$ side while the slower component is left behind and becomes enriched at the low-$p(O_2)$ side.

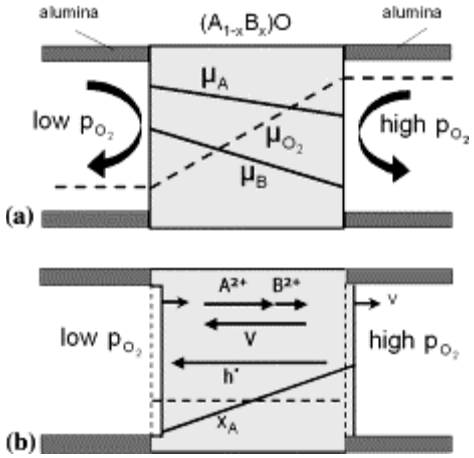

Fig. 2.1 Oxide $A_{1-x}B_xO$ exposed to the oxygen potential gradient. (a) Chemical potential gradients of chemical components A, B and O; (b) fluxes of cations, A^{2+} and B^{2+}, cation vacancies, V, and electron holes, $h^{\bullet}$.[6]

When the cations and cation vacancies arrive at the crystal surfaces the chemical reactions occur.[6] At the high-$p(O_2)$ side, cations, A^{2+}, are oxidized by the oxygen from the gas phase according to the following reaction

$$A_A^X + \frac{1}{2}O_2(g) \rightarrow V_A^{//} + 2h^{\bullet} + AO \quad (1)$$

At the low-p(O_2) side the opposite reaction takes place and the oxide anions are reduced to the oxygen according to the following reaction

$$V_A^{//} + 2h^{\bullet} + BO \rightarrow B_A^X + \frac{1}{2}O_2(g) \quad (2)$$

As a consequence, the oxide surfaces shift to the side of higher oxygen potential. In summary, the external oxygen potential causes:[6]

1. The directed flux of cation vacancies from the high to the low oxygen potential side of the oxide.
2. The drift motion of both crystal surfaces towards the high-p(O_2) side.
3. A demixing of cations with enrichment of the faster cation at the high-p(O_2) side.

The stability and durability of functional oxides for solid oxide fuel cells and gas separation membranes are one of the main technical challenges.[2] The understanding of stability issues requires the knowledge of transport properties and defect chemistry of these materials. The chemical diffusion of mobile components of oxides occurs due to the exposure to chemical potential gradients. Diffusion coefficient is a fundamental property for each component of the oxide.[7] The diffusion coefficients of the anions in the perovskite-type oxides are mostly higher than the diffusion coefficients of the cations.[8] The cation mobility is, therefore, probably the rate-limiting step in the materials degradation. Once the chemical diffusion coefficient of a rate limiting species is known, the durability of the high temperature device can be estimated. The relationship between the diffusion length, *x*, and the diffusion time, *t*, can be given in a first approximation as $t = bx^2 / D$, where D is the diffusion coefficient and b is a constant in order of 1.[7] The diffusion times, computed as $t = x^2 / D$, for the typical cation diffusion coefficients at high temperatures are given in Table 2.1. It is apparent already from this rough estimation that the role of cation diffusion becomes significant as soon as the diffusion length reaches 10 – 100 μm. Since it is desirable to reduce the thickness of electrolytes for SOFC and oxygen permeable membranes,[9] the materials selection needs to be made with respect to the diffusion coefficients of the least mobile species. It is the objective of the present work to study the cation diffusion in $LaMnO_3$, $LaCoO_3$ and $LaFeO_3$ materials by three different techniques, determine diffusion coefficients and contribute further to the general understanding of mass transport processes and defect chemistry of these oxides.

Table 2.1 Estimated diffusion times for several diffusion coefficients and diffusion lengths.

x	D/ cm^2s^{-1}		
	10^{-10}	10^{-11}	10^{-12}
1 cm	318 y[a]	3 180 y	31 800 y
1 mm	3.18 y	31.8 y	318 y
100 μm	1.65 w	16.5 w	3.18 y
10 μm	2.8 h	28 h	280 h
1 μm	100 s	1 000 s	10 000 s
1 nm	0.1 ms	1 ms	10 ms

[a]y = year, w = week, h = hour, s = second, ms = millisecond

References

1. Minh, N. Q. *J. Am. Ceram. Soc.* **1993**, *76*, 563.
2. Antoni, L. *Mater. Sci. Forum* **2004**, *461-464*, 1073.
3. Fontaine, M. L.; Larring, Y.; Norby, T.; Grande, T.; Bredesen, R. *Ann. Chim.* **2007**, *32*, 197.
4. Bouwmeester, H. J. M. *Catal. Today* **2003**, *82*, 141.
5. Balachandran, U.; Dusek, J. T.; Mieville, R. L.; Poeppel, R. B.; Kleefisch, M. S.; Pei, S.; Kobylinski, T. P.; Udovich, C. A.; Bose, A. C. *Appl. Catal. A* **1995**, *133*, 19.
6. Martin, M. *J. Chem. Thermodyn.* **2003**, *35*, 1291.
7. Kirkaldy, J. S.; Young, D. J. *Diffusion in the condensed state*, The Institute of Metals: London, Great Britain, 1987.
8. Islam, M. S. *J. Mater. Chem.* **2000**, *10*, 1027.
9. Hendriksen, P. V.; Larsen, P. H.; Mogensen, M.; Poulsen, F. W.; Wiik, K. *Catal. Today* **2000**, *56*, 283.

3. Introduction

3.1. Perovskite structure

The perovskite structure bears its name after the mineral with the same composition, $CaTiO_3$.[1,2,3] The general formula unit of the perovskite is ABX_3 where A is a larger cation, B is a smaller cation and X is an anion. The ideal perovskite structure is cubic. The B cations are located in the corners of the cube and the A cation occupies the centre of the cube. The anions are located at the cube edges, between two B cations. Each B cation is surrounded by six anions and forms the centre of the BX_6 octahedra. The BX_6 octahedras extend infinitely in three dimensions. The perovskite structure is given in Fig. 3.1.[1,2] The perovskite structure can also be regarded as a superstructure of the ReO_3-type that has, in addition, the A cations occupying the cavities (Fig. 3.1b).

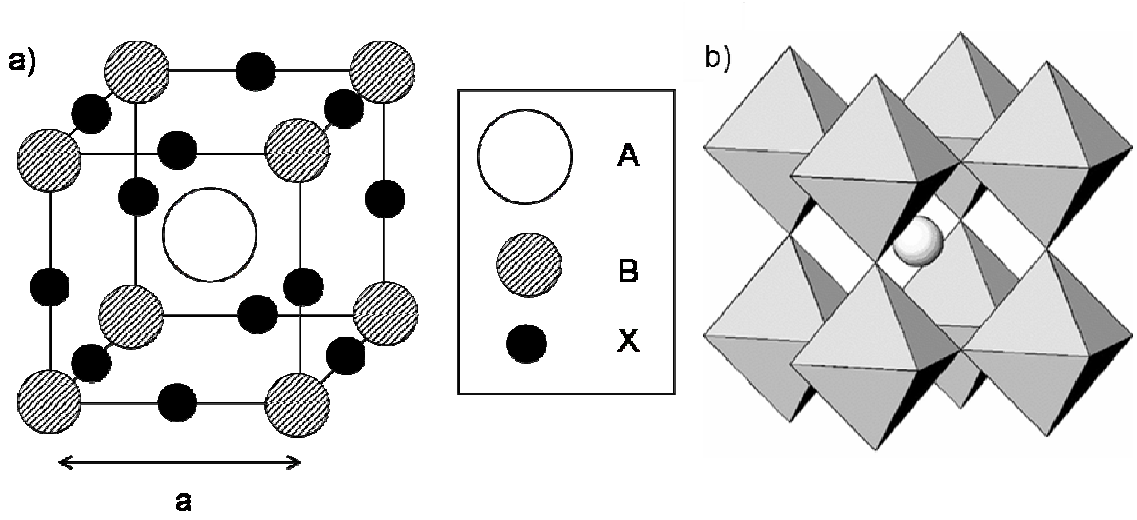

Fig. 3.1 The ideal cubic perovskite structure.

In the ideal perovskite structure, the B-X distance, r_{B-X}, is equal to a/2 and the A-O distance, r_{A-X}, is equal to $a/\sqrt{2}$ where a is a cubic unit cell parameter (Fig. 3.1a). A useful parameter, *t*, can be defined by the ratio between A-X and B-X distances[1]

$$t = \frac{r_{A\text{-}X}}{\sqrt{2}\, r_{B\text{-}X}} = \frac{r_A + r_X}{\sqrt{2}\,(r_B + r_X)} \qquad (3.1)$$

where r_A, r_B and r_X are the respective effective ionic radii. t is the Goldschmidt tolerance factor.[4] The ideal cubic perovskite structure has $t = 1$. It was observed, however, that the perovskite structure remains preserved also when *t* is smaller or larger than 1, in fact $0.75 < t < 1.05$.[3] Nevertheless, the structure becomes distorted and less symmetric. The reduction

in symmetry is driven by the necessity to accommodate the anion coordination number around the cations. One or more of the following processes usually happen:[5,6,7]

1. Titling of the anion octahedra
2. Displacement of the cations
3. Distortion of the octahedra

These structural distortions were studied in detail by Glazer in 1970s.[5,6] Glazer provided a classification of lattice distortions of perovskites and described 23 different tilt systems.[5] It is out of the scope of the present work to discuss all structural types of the perovskites. In the following, we shall provide only a brief description of the structures and known structural transitions of $LaMnO_3$, $LaCoO_3$ and $LaFeO_3$ materials since they are the subject of the present study.

Lanthanum manganite, $LaMnO_3$, t ~ 0.95, possess both the cation and oxygen nonstoichiometry.[8] A rhombohedral symmetry with space group $R\bar{3}c$ is found for $LaMnO_{3+\delta}$ where $0.10 \leq \delta \leq 0.18$.[9] For $\delta < 0.10$, two orthorhombic structures with the space group Pnma are found: ORT1-type with a Jahn-Teller distorted octahedra and ORT2-type with a regular MnO_6-octahedra.[10,11] The Jahn-Teller distortion occurs due to the high-spin state of Mn^{3+} cations.[9] The lanthanum deficiency, x, in lanthanum manganite, $La_{1-x}MnO_{3+\delta}$, determines, in addition to the temperature and oxygen partial pressure, the stability region for different crystal symmetries. The phase stability regions can be found in ref. 10.

Lanthanum cobaltite, $LaCoO_3$, has a rhombohedrally distorted perovskite lattice with the space group $R\bar{3}c$.[12] It transforms to the ideal cubic lattice at ~ 1610 K.[13] Two other structural changes are observed at 100 K and 500 K.[14,15] These transformations are observed due to the transition from the low spin state (t_{2g}^6) to the intermediate spin state ($t_{2g}^5 e_g^1$) and then to the high spin state ($t_{2g}^4 e_g^2$).[14] These spin transitions are accompanied by a large increase of the ionic radius of Co^{3+}, from 0.545 Å to 0.61 Å.[14,15]

Lanthanum ferrite, $LaFeO_3$, crystallises in the orthorhombic space group Pbnm at temperatures below ~ 1273 K.[16] At temperatures above 1273 K, it has a rhombohedral structure with space group $R\bar{3}c$.[17]

Beside the ionic radii requirement (3.1), the electroneutrality condition in perovskite-type oxides has to be satisfied. If $X = O^{2-}$, the following charge distributions between A and B cations are allowed: $A^{1+}B^{5+}O_3$, $A^{2+}B^{4+}O_3$, $A^{3+}B^{3+}O_3$.[2,3] A partial substitution of A or B cations is also allowed. The possibility to partially substitute cations in the perovskite structure leads, therefore, to an extremely large number of perovskite compounds with variable properties.[18] Applications of these compounds in science and technology are wide-ranging and have been a subject of several reviews, including ref. 1, 2, 3 and 18.

3.2. Heterogeneous phase equilibria and nonstoichiometry of $LaMnO_3$, $LaCoO_3$ and $LaFeO_3$ materials

The $LaMnO_3$ perovskite system exhibits a well-established oxygen nonstoichiometry. The oxygen content measured at 1273 – 1473 K is given in Fig. 2.[19] The $LaMnO_3$ compound exhibits an oxygen excess as well as an oxygen deficiency depending on the experimental conditions. The oxygen deficiency is strongly dependent on temperature (Fig. 3.2). In addition to the oxygen nonstoichiometry, this compound has also a significant deviation from the cation molar ratio 1:1.[20] The well-established nonstoichiometry makes the defect chemistry of $LaMnO_3$ more complicated relative to $LaCoO_3$ and $LaFeO_3$ materials. The phase diagram of the pseudo-binary system La_2O_3 – Mn_2O_3 was first reported by van Roosmalen et al.[20] A. N. Grundy et al. recently provided a defect model that best suits the experimental observations in air.[21] This model includes anti-site defects - Mn^{3+} cations occupying vacant La sites and also a possibility of Mn to exist in several oxidation states. The following sublattice occupation for $LaMnO_3$ was adapted: $(La^{3+}, Mn^{3+}, Va)_1(Mn^{2+}, Mn^{3+}, Mn^{4+}, Va)_1(O^{2-}, Va)_3$ where Va represents a vacant site.[21] Vacancies at all three sublattices are present in $LaMnO_3$. The calculated pseudo-binary diagram of the La_2O_3 – Mn_2O_3 system in air is given in Fig. 3.3.[21] Experimental observations of cation nonstoichiometry were included for a comparison. The agreement between the experimental data and calculations was good. A. N. Grundy et al. also calculated the phase diagram of the La_2O_3 – Mn_2O_3 system at $p(O_2)$ = 1 Pa.[21] It was predicted that the solid solubility region of $LaMnO_3$(ss) becomes narrower with $p(O_2)$ and that the composition at the $LaMnO_3$-MnO phase boundary shifts towards a Mn-deficiency at low temperatures. We will show in Paper I how this model fits with our experimental observations from reactive diffusion couples La_2O_3 – Mn_3O_4 measured at 1370 – 1673 K and $p(O_2)$ = 40 Pa – 50 kPa, where also a further discussion of the defect chemistry of $LaMnO_3$(ss) will be provided.

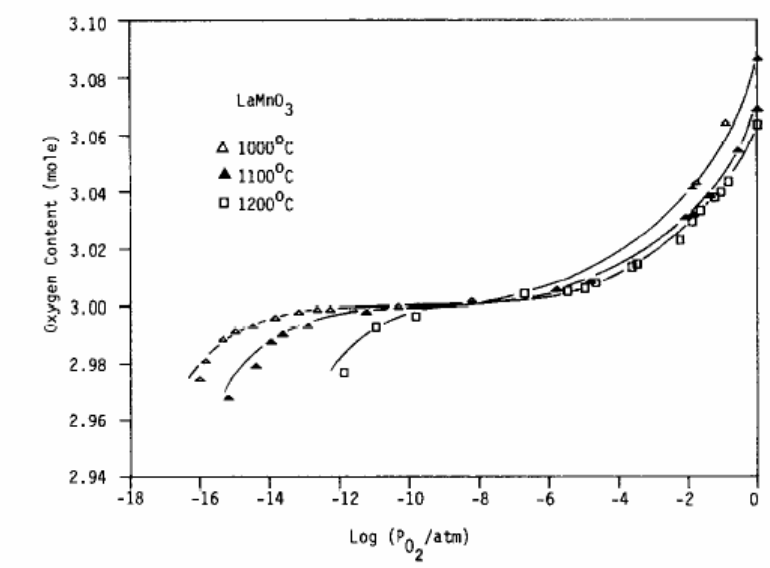

Fig. 3.2 Oxygen content in $LaMnO_3$ measured at different temperatures and oxygen partial pressures.[19]

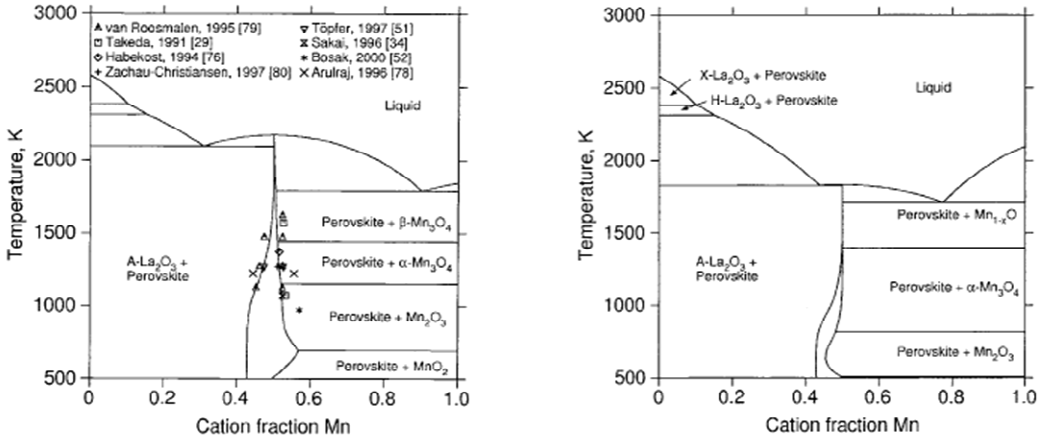

Fig. 3.3 Pseudobinary phase diagram of the La_2O_3 – Mn_2O_3 system in air (left) and at $p(O_2)$ = 1 Pa. Experimental observations of cation nonstoichiometry are also included.[21]

$LaCoO_3$ exhibits a well-established oxygen deficiency and may, therefore, be written as $LaCoO_{3-\delta}$.[22] A plot of oxygen deficiency, δ, for several temperatures and oxygen partial pressures is given in Fig. 3.4.[22] It was suggested that the oxygen nonstoichiometry may be explained by a random defect model.[23] The defects in $LaCoO_{3-\delta}$ are formed due to the following two defect equilibria

$$O_O^X + 2Co_{Co}^{\bullet} = V_O^{\bullet\bullet} + 2Co_{Co}^X + \frac{1}{2}O_2 \qquad (3.2)$$

$$2Co_{Co}^{X} = Co_{Co}^{\bullet} + Co_{Co}^{/} \quad (3.3)$$

and the point defects are randomly distributed in the material. The comparison between the observed and calculated oxygen deficiency is provided in Fig. 3.5.[23] The agreement between the experimental and calculated oxygen deficiency was good.

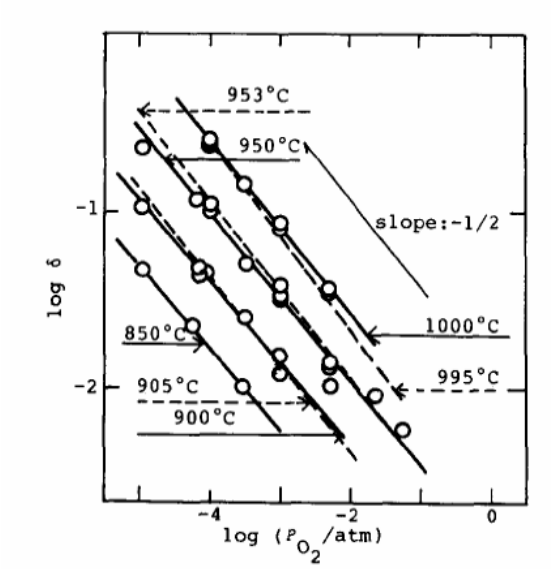

Fig. 3.4 Oxygen deficiency, δ, in $LaCoO_{3-\delta}$ at several temperatures and oxygen partial pressures.[22]

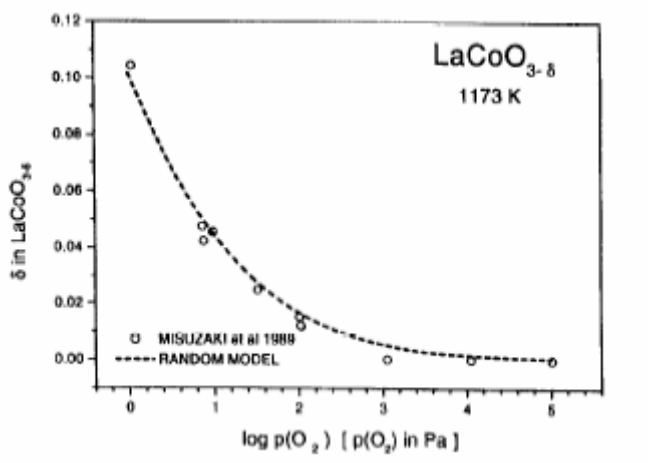

Fig. 3.5 Comparison between calculated and experimentally observed oxygen deficiency in $LaCoO_{3-\delta}$.[23]

Due to the pronounced oxygen deficiency the $LaCoO_{3-\delta}$ phase is unstable at low oxygen partial pressures. Two other ternary phases, $La_4Co_3O_{10}$ and La_2CoO_4, have been reported to be present at reducing conditions.[24-26] These phases have a crystal structure of the Ruddlesden-Popper type, $La_{n+1}Co_nO_{3n+1}$, which can be described as an alternation of n perovskite layers with rock salt layers.[26] An isothermal cross-section of the phase diagram for the La-Co-O system is given in Fig. 3.6.[26] The stability region of the $La_4Co_3O_{10}$ phase is narrow in comparison with the stability regions of the $LaCoO_{3-\delta}$ and La_2CoO_4 phases. The phase equilibria in the La-Co-O system will be discussed further with respect to the reactive diffusion couples of La_2O_3 – CoO phases in Paper II of this thesis.

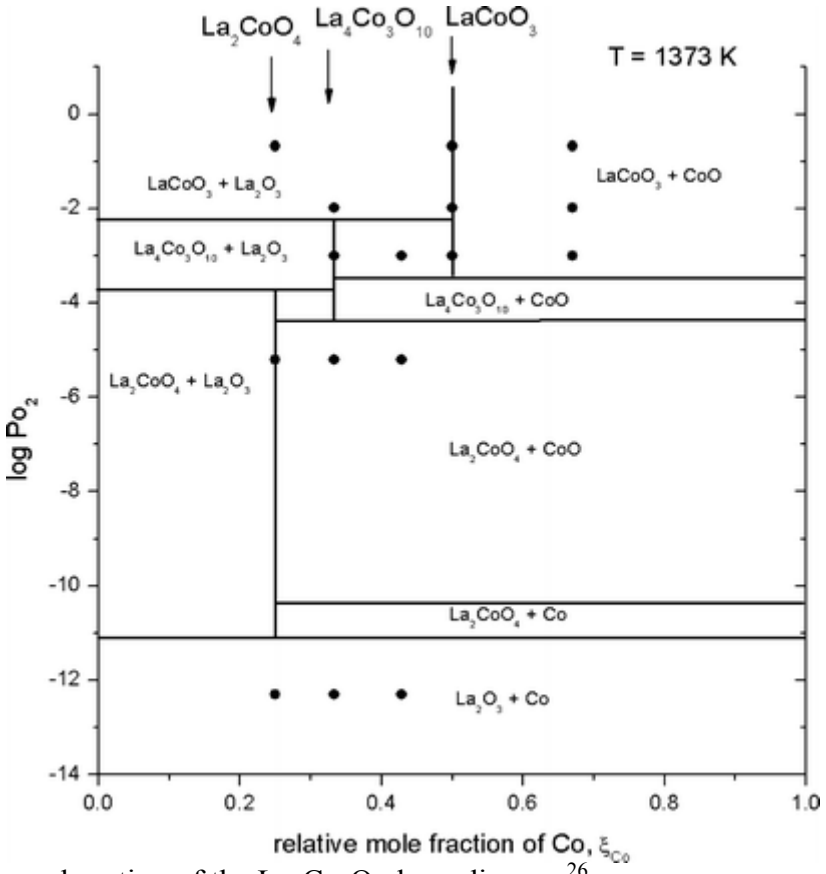

Fig. 3.6 Isothermal section of the La-Co-O phase diagram[26]

Pure $LaFeO_3$ have a very narrow homogeneity range.[27,28] It becomes oxygen deficient at a significantly lower oxygen partial pressure compared to $LaCoO_3$.[27] The phase diagram of the pseudo-binary La_2O_3 – Fe_2O_3 system is given in Fig. 7.[29] Beside the $LaFeO_3$ phase, only one other ternary compound was found, $LaFe_{12}O_{19}$. This phase is ferromagnetic and 1/12 of the iron is in the ferrous state. The $LaFe_{12}O_{19}$ phase decomposes to $LaFeO_3$ and Fe_3O_4 at 1694 K.[29]

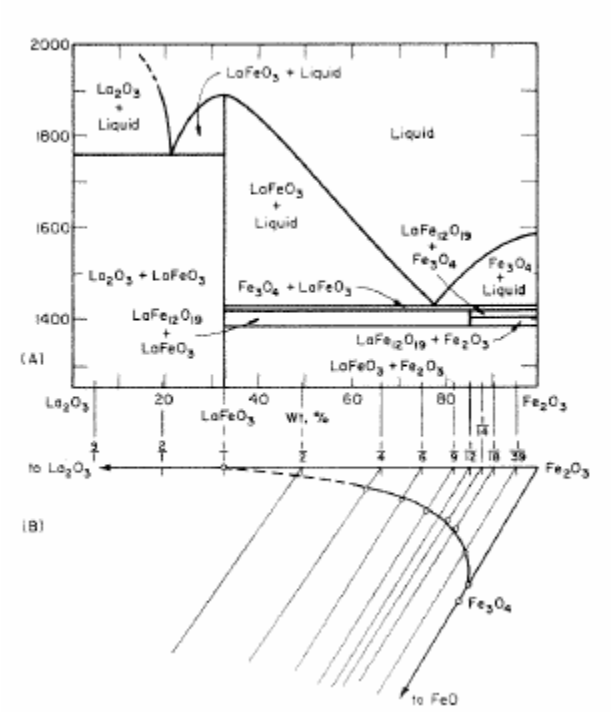

Fig. 3.7 Phase diagram of the La_2O_3 – iron oxide system in air. Temperature is given in °C.[29]

3.3. Cation diffusion in $LnBO_3$ perovskite-type oxides – theoretical considerations

It is now well established that the mass transport processes in crystalline oxides proceed by the means of point defects.[30] There are two basic mechanisms - vacancy and interstitial diffusion.[31] These two features are similar to diffusion processes in other crystalline materials - metals and intermetallic compounds. The main differences between oxides and metals with implications to diffusion processes are the following:[32]

1. Most oxides are ionic compounds. They consist of cations and anions with well defined, opposite charges.
2. Crystalline oxides consist of two or more sublattices. Due to the opposite charges of the cations and anions, the cation diffusion takes place in the cation sublattice(s) and the anion diffusion takes place in the anion sublattice.
3. The concentration of point defects, in addition to intensive thermodynamic variables such as temperature and pressure, depends also on the chemical potential of oxygen.
4. Diffusion processes in oxides may be facilitated by a parallel diffusion of electrons and holes since oxides may be electrically conducting.
5. The crystal structure influences the defect structure of the oxide.

From the structural point of view, the interstitial positions in the perovskites are not favoured due to the close atomic packing. It is, therefore, probable that the cation diffusion

takes place mostly by a vacancy migration mechanism. The A cations in perovskite lattice may be totally missing without the collapse of the BO_6-network. The B site vacancies in perovskites, on the other hand, are not favoured since the BO_6 octahedras form the backbone of the perovskite structure. The vacancy diffusion taking place only in the B cation sublattice itself would be complicated since an oxygen anion is located between two neighbouring sites. The oxygen ion transport in several $LaBO_3$ oxides has already been studied by both the experimental and theoretical methods. Data are compared in Table 3.1.[32] The reproducibility of the oxygen ion vacancy migration energies with experimental values was good.[32] For this reason, we shall deal with the theoretical results first to get an insight into the ionic transport in $LaBO_3$-type oxides. These studies are useful since they provide an atomistic approach into cation diffusion. Experimental cation diffusion studies will be discussed later.

Table 3.1 Calculated and experimental oxygen vacancy migration energies in $LaBO_3$ oxides (1 eV ≐ 96.5 kJ mol^{-1}).[32]

Cmpd.	E_m / kJ mol^{-1}	
	Calc.	Exp.
$LaGaO_3$	70.4	76.2, 63.7, 70.2
$LaMnO_3$	83.0	70.4
$LaCoO_3$	58.9	56.0, 75.3
$LaYO_3$	117.7	125.5

The formation and migration of cation defects was studied in detail for $LaMnO_3$ by De Souza et al.[33] To the present date, there have not been published any reports in the literature dealing with the direct experimental determination of cation diffusion coefficients in this perovskite system. The calculations of cation defect energies in $LaMnO_3$ were based upon the Born model of ionic solids with ions assigned integral charges corresponding to their formal oxidation states.[33] The calculation of defect formation and migration energies utilised the Mott-Littleton approach in which the crystal lattice was split into two regions. The first region was spherical with the defect in its centre and consisted of 150 – 200 ions. The emphasis in calculations was placed on the local lattice relaxation around the defect.[33] The second region, the remaining crystal, was the region where forces due to defect were relatively weak and the response could be, therefore, treated by more approximate quasi-continuum methods. The migration energy of the ion was determined by calculating the defect energy of the migrating ion at different positions along the migration path.[33]

The formation energies of isolated vacancies and interstitial defects were computed for the rhombohedral and orthorhombic structures. The interstitial defect was represented by an octahedral interstice situated at the position $(0,0,1/2)_{cubic}$. Calculated values are listed in Table 3.2.[33] For both systems the cation Frenkel disorder energies are much higher than the other disorder energies. It can, therefore, be concluded that the vacancies and not the interstitials will be the dominant structural defects. The effect of structural distortion on

cation disorder energies is about 10 %. The effect of structural distortion on oxygen Frenkel disorder energies is negligible.

Table 3.2 Calculated energies for Frenkel disorder, partial and full Schottky disorder in $LaMnO_3$ crystals.[33]

		Energy per defect / kJ mol^{-1}	
Name	Reaction	Rhombohed.	Orthoromb.
La Frenkel	$La_{La}^{X} \rightarrow V_{La}^{///} + La_{i}^{\bullet\bullet\bullet}$ [a]	973	893
Mn Frenkel	$Mn_{Mn}^{X} \rightarrow V_{Mn}^{///} + Mn_{i}^{\bullet\bullet\bullet}$	848	887
O Frenkel	$O_{O}^{X} \rightarrow V_{O}^{\bullet\bullet} + O_{i}^{//}$	388	386
$LaMnO_3$ full Schottky	$nil \rightarrow V_{La}^{///} + V_{Mn}^{///} + 3V_{O}^{\bullet\bullet} + LaMnO_3^{surf}$	336	360
La_2O_3 partial Schottky	$nil \rightarrow 2V_{La}^{///} + 3V_{O}^{\bullet\bullet} + La_2O_3^{surf}$	309	338
Mn_2O_3 partial Schottky	$nil \rightarrow 2V_{Mn}^{///} + 3V_{O}^{\bullet\bullet} + Mn_2O_3^{surf}$	359	380

[a]standard Kröger-Wink notation was used

Upon the examination of the perovskite structure (Fig. 3.1) it is apparent that the obvious vacancy migration path for La vacancy is the $(100)_{cubic}$ direction. Calculated vacancy migration energies are listed in Table 3.3.[33] The La vacancy can exchange its position with one of the six surrounding La cations. All six jump distances are equal in the cubic and rhombohedral perovskite structures. In the orthorhombic structure there are three different jump distances and, therefore, three different migration energies. The saddle point configuration consisted of the migrating La cation moving through the aperture defined by four oxygen anions.[33] Four oxygen anions provided a severe steric hindrance to the A site migration. The radius of the sphere that would just pass through the aperture was, in fact, similar to the radius of the B site cation. Since La^{3+} was larger, the surrounding lattice had to relax substantially to allow the A site cation to migrate. The shortest oxygen-oxygen separation distances across the octahedral interstice are, therefore, also included in Table 3.3 for the comparison.[33] As expected, vacancy migration energy increases as the separation distance decreases.

Table 3.3 Calculated activation energies for La vacancy migration, E_m^{La}, and shortest oxygen-oxygen separation distances across the octahedral interstice, d_{O-O}^{oct}, in $LaMnO_3$.[33]

	E_m^{La} / kJ mol^{-1}	d_{O-O}^{oct} / Å
Cubic	379	3.904
Rhombohedral	400	3.481
Orthorombic	407	3.469
	411	3.415
	417	3.406

Two migration paths for Mn vacancy were investigated in detail. These are illustrated in Fig. 3.8.[33] The calculated migration energies are given in Table 3.4.[33] The first path involved jumps of individual Mn cations along the diagonal. In this case, the Mn cation did not have an oxygen anion directly in its way. Nevertheless, the calculated migration energies for the migration path A were extremely high.[33] This is due to the fact that the jumping Mn^{3+} cation was surrounded by two apical La cations. The main reason for such high migration energies was attributed to the electrostatic repulsion between Mn^{3+} and La^{3+} cations. The second possible migrating path was also investigated. In this case, the migrating Mn^{3+} cation moved up and around the oxygen anion located between two neighbouring Mn sites. The authors believed that this transport path represented a balance between the repulsive cation interactions and the large displacement which the oxygen ion must undergo. Calculated migration energies were lower.

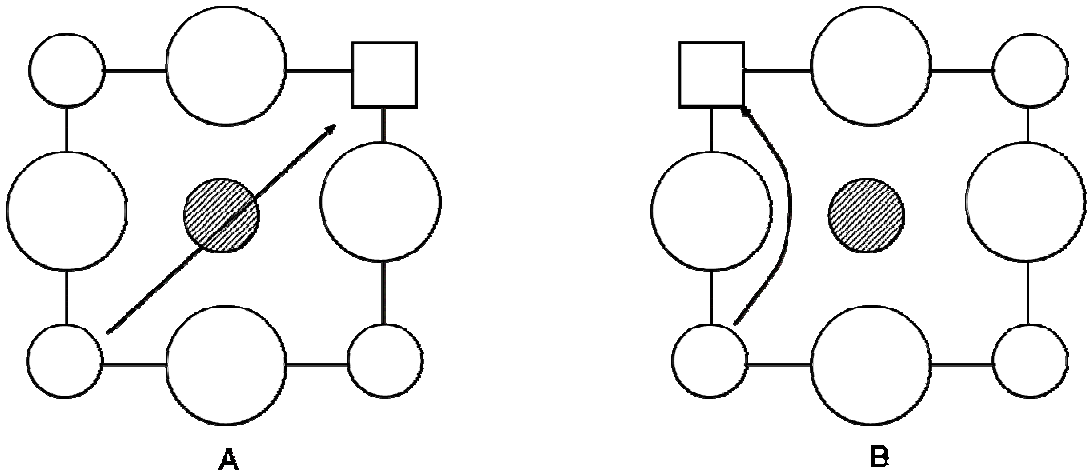

Fig. 3.8 Possible jumping mechanisms for Mn^{3+} cations in $LaMnO_3$ investigated in ref. 22 projected to the $(100)_{cubic}$ plane. Mn cations are represented by small open circles, Mn vacancies by small open squares, oxygen anions by large open circles, La cations by line-shaded circles. La cations are situated above and behind the plane given by Mn and O ions.

Table 3.4 Calculated activation energies for manganese vacancy migration in $LaMnO_3$[33]

	E_m^{Mn} / kJ mol^{-1}	
	Mechanism A	Mechanism B
Cubic	1420	746
Rhombohedral	1351; 1518	851
Orthrombic	1362; 1421	959; 1027

Finally, the authors preliminarily investigated the effect of a removal of a neighbouring La^{3+} cation in the transition state. The location of Mn^{3+} cations at vacant La positions was experimentally confirmed. Preliminary calculations of manganese vacancy migration mediated by lanthanum vacancies yielded a value for Mn^{3+} migration energy ca. 3.5 eV

(340 kJ mol^{-1}).[33] It is apparent already from these simulations that the lanthanum vacancy concentration could be an important parameter since it would explicitly determine not only the lanthanum diffusion coefficient but also the manganese diffusion coefficient and thus, the overall cation transport properties of $LaMnO_3$.

Atomistic simulations based on Mott-Littleton calculations have also been performed for $LaGaO_3$.[34] The activation energies for cation self-diffusion were nearly identical to the values obtained for $LaMnO_3$. This reflects comparable ion-ion interactions in $LaBO_3$ perovskites. Migration energies for selected A site cations on the La^{3+} and Ga^{3+} sublattices were also calculated and these are given in Table 3.5.[34] It can be seen that the transport of divalent cations at the La and Ga sublattices is easier than the transport of trivalent cations. This is due to the decrease in repulsive interactions between positively charged ions. Also, the transport of smaller cations in the La sublattice is easier since they can better fit into the aperture formed by O^{2-} anions. In the $LaGaO_3$ study it was, again, pointed out that the B cation diffusion could be significantly facilitated by the presence of La vacancies.

Table 3.5 Calculated migration energies (in kJ mol^{-1}) for cation self-diffusion and impurity diffusion on the La^{3+} and Ga^{3+} sublattices in $LaGaO_3$.[34]

	La sublattice	
Cation	Pseudo-cubic	Orthrombic
La^{3+}	436	455; 457; 455
Sm^{3+}	347	386; 386; 383
Gd^{3+}	311	354; 356; 354
Ba^{2+}	366	371; 373; 372
Sr^{2+}	258	267; 267; 267
	Ga sublattice	
	Mechanism A	Mechanism B
Ga^{3+}	1370	754
Sc^{3+}	1304	*
Fe^{3+}	1352	839
Cr^{3+}	1420	795
Al^{3+}	1389	*
Co^{2+}	969	609
Zn^{2+}	948	663
Mg^{2+}	997	644

* transition state not found

Neither the presence of electronic defects (holes) that could facilitate the cation transport nor the effect of surrounding cation vacancies on the cation diffusion were investigated in the atomistic simulations. The diffusion in the Mott-Littleton calculations is generally calculated in a well-defined surrounding, free of further disorder.[33,34] The properties of heavily disordered systems are, therefore, difficult to calculate. Molecular dynamics (MD) has an advantage that absolute diffusion coefficients can be calculated at

various temperatures and then be compared to experimental values. Nevertheless, only relatively fast processes such as oxygen diffusion can be modelled due to the limited computer time.[35,36] Kilo et al. performed the MD studies on cation diffusion in heavily disordered systems like strontium and magnesium doped lanthanum gallate ($La_{0.9}Sr_{0.1}Ga_{0.9}Mg_{0.1}O_{2.9}$, LSGM) and yttria-stabilised zirconia (YSZ) for the first time.[37] To overcome problems, a well-defined concentrations of cation vacancies were artificially introduced into simulation boxes and their behaviour was modelled using long-time calculation runs.[37] The influence of defect concentration was estimated using varying defect concentrations. It was found that the diffusion of all the cations in LSGM is correlated and occurs via two neighbouring vacancies on the A and B sites of the perovskite lattice.[37] These two vacancies migrate together and form a binary vacancy complex. A cations hop directly to the neighbouring A site vacancies while B cations are allowed to use an A site vacancy as an intermediate state. This leads to the similar cation diffusion coefficients for all four types of cations and explains the experimental observations for $La_{0.9}Sr_{0.1}Ga_{0.9}Mg_{0.1}O_{2.9}$.[38]

3.4. Cation diffusion in $LnBO_3$ perovskite-type oxides – experimental observations

Experimental studies on cation diffusion in perovskite-type oxides of the $LnBO_3$ type (Ln = La or lanthanoid cation, B = transition metal element) are relatively scarce in the literature. Freer in his review of self-diffusion and impurity diffusion data in oxides published in 1980 provided data only for one perovskite compound – $NdFeO_3$.[39] The need for new experimental studies is, therefore, apparent. The cation diffusion has experimentally been studied directly (tracer diffusion and inter-diffusion experiments) and indirectly (following the kinetics of a process explicitly limited by cation diffusion). Table 3.6 contains experimental data available on cation diffusion in unsubstituted $LnBO_3$ oxides.[40-51] Experimental activation energies are in a large range of ~ 50 – 600 kJ mol^{-1}, depending on the cation, material and experimental technique used. These values are mostly lower than predictions of activation energies from atomistic simulations. In the following discussion we will discuss differences in the activation energy that may arise from the use of different experimental techniques. A further discussion of the activation energies will also be later provided in research papers of this thesis.

Activation energies resulting from reactive diffusion couple experiments are higher than activation energies from tracer diffusion experiments. It was suggested that this could be due to the nature of the experimental methods used.[41,50] In reactive diffusion measurements it is likely that a new perovskite phase, which is continuously formed, contains an equilibrium population of cation vacancies. The activation energy is, therefore, probably a sum of activation energies for vacancy formation and migration respectively. In tracer diffusion experiments, the population of cation vacancies might have already been defined by the sintering temperature during the material's synthesis.[38] The concentration of vacancies probably exhibit only minor changes with annealing temperature. If so, activation energies obtained from tracer diffusion experiments reflect only the activation barrier for

jumps between lattice sites. One could, therefore, evaluate directly the activation energy for vacancy migration and formation from these two diffusion experiments. This hypothesis, however, needs to be experimentally tested by diffusion experiments involving the same cation. To the best of our knowledge, only one system – Co^{3+} diffusion in $LaCoO_3$ – was studied by both experimental methods.[43,49] Tracer diffusion experiments most often involve diffusion studies of an impurity element. Some metals, including manganese or cobalt, have only one stable, naturally occurring isotope. Alternative choices, therefore, need to be sought. Small amount of radioactive isotopes could be a possibility to overcome this problem, as reported by Petrov et al.[43] and Pavlyuchenko et al.[42] in their studies of $LnCoO_3$ and $LnFeO_3$ materials.

Table 3.6 Experimental data available on cation diffusion in unsubstituted $LnBO_3$ oxides[40-50]

Compound	Cation	T / K	E_A / kJ mol^{-1}	Reference
Tracer and radiotracer diffusion experiments				
$YCrO_3$	La^{3+}	1273 - 1473	*	Hong et al. (2001)[40]
$YCrO_3$	Mn^{3+}	1273 - 1473	*	Hong et al. (2001)[40]
$LaFeO_3$	Y^{3+}	1173 - 1373	*	Wærnhus et al. (2004)[41]
$LaFeO_3$	Cr^{3+}	1173 - 1373	*	Wærnhus et al. (2004)[41]
$NdFeO_3$	Nd^{3+}	1513 - 1693	80	Pavlyuchenko et al. (1970)[42]
$NdFeO_3$	Fe^{3+}	1513 - 1693	93	Pavlyuchenko et al. (1970)[42]
$LaCoO_3$	Co^{3+}	1273 - 1523	170 ± 15	Petrov et al. (1987)[43]
$PrCoO_3$	Co^{3+}	1273 - 1523	182 ± 8	Petrov et al. (1987)[43]
$NdCoO_3$	Co^{3+}	1273 - 1523	163 ± 6	Petrov et al. (1987)[43]
$SmCoO_3$	Co^{3+}	1273 – 1523	107 ± 4	Petrov et al. (1987)[43]
$EuCoO_3$	Co^{3+}	1273 – 1523	79 ± 6	Petrov et al. (1987)[43]
$GdCoO_3$	Co^{3+}	1273 – 1523	50 ± 6	Petrov et al. (1987)[43]
$PrCoO_3$	Pr^{3+}	1273 – 1523	75 ± 6	Petrov et al. (1987)[43]
$SmCoO_3$	Sm^{3+}	1273 – 1523	148 ± 15	Petrov et al. (1987)[43]
$EuCoO_3$	Eu^{3+}	1273 - 1523	117 ± 11	Petrov et al. (1987)[43]
$LaGaO_3$	Fe^{3+}	1673	*	Matraszek et al. (2002)[44]
$LaGaO_3$	Cr^{3+}	1673	*	Matraszek et al. (2002)[44]
$LaGaO_3$	Y^{3+}	1673	*	Matraszek et al. (2002)[44]
Inter-diffusion couples				
$LaFeO_3$	Nd^{3+}	1373 - 1573	610 ± 30	Smith et al. (2006)[45]
$NdFeO_3$	La^{3+}	1373 - 1573	610 ± 30	Smith et al. (2006)[45]
Reactive diffusion couples				
$LaCrO_3$	La^{3+}	1483 - 1695	480	Akashi et al. (1998)[46]
$NdCrO_3$	Nd^{3+}	1473 - 1773	343	Akashi et al. (2001)[47]
$YCrO_3$	Y^{3+}	1458 - 1719	272	Kawamura et al. (1995)[48]
$LaCoO_3$	Co^{3+}	1523 - 1573	550 ± 20	Petrov et al. (1981)[49]
$LaFeO_3$	Fe^{3+}	1223 - 1623	320 ± 20	Smith et al. (2006)[50]

* Activation energy not reported

The absolute values of cation diffusion coefficients in the perovskite-type oxides are observed in the range of $10^{-8} – 10^{-18}$ cm^2s^{-1}. The data are given in Fig. 3.9. The values are spread over 10 orders of magnitude. The grain boundary diffusion coefficients are usually about 5 orders of magnitude higher than the respective bulk diffusion coefficients. The grain boundaries constitute a rapid transport path in these materials. A cation enrichment at the grain boundaries was also confirmed by other, independent techniques.[56,57] The reactive diffusion couples often provide information about the self-diffusion of the faster cation. The complementary studies are, therefore, needed to obtain information about the least mobile cations. Tracer diffusion studies are most often performed with impurity elements. Information regarding the chemical self-diffusion of the least mobile species is, therefore, very often lacking. $LaFeO_3$ is one of the compounds where the lower mobility of La^{3+} relative to Fe^{3+} was confirmed with separate inter-diffusion coples of $LaFeO_3 – NdFeO_3$.[45]

Further experimental data available on cation diffusion involve substituted perovskite compounds.[38,41,44,51-55] The influence of dopant fraction on cation diffusion was studied in detail for $La_{1-x}Sr_xGa_{1-x}Mg_xO_{3-z}$.[44] Three elements, Fe, Cr and Y, respectively, were studied. It was found that the diffusion coefficients passed through a minimum at x = 0.02 but the values of diffusion coefficients were nearly identical.[44] The effect of the substitution was also studied by I. Wærnhus et al. for $La_{1-x}Sr_xFeO_3$.[41] It was observed that the substitution level did not have a dramatic effect on cation diffusion coefficients.

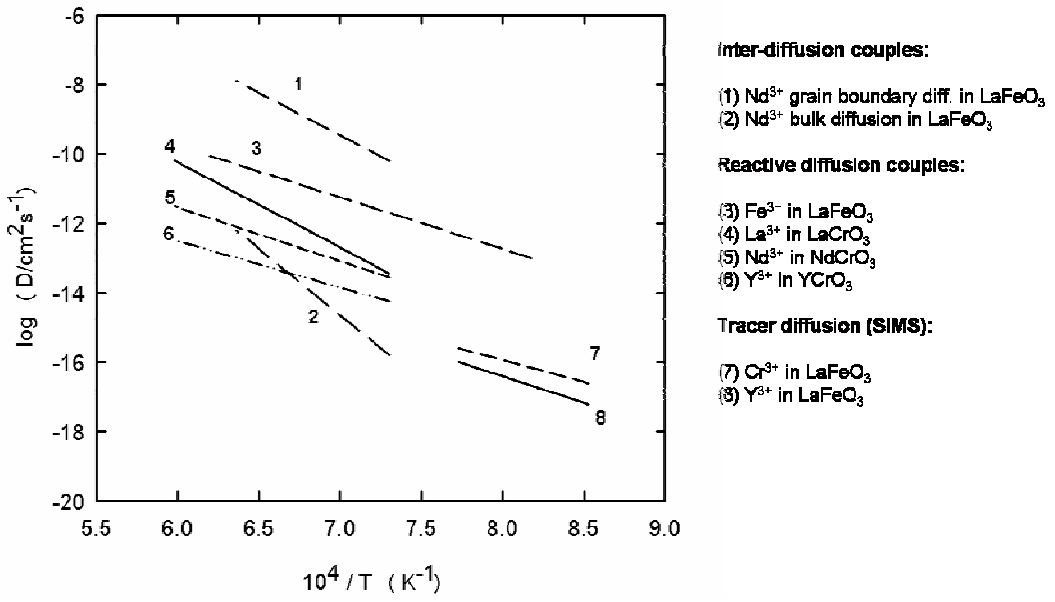

Fig. 3.9 Cation diffusion in unsubstituted perovskite oxides.

The cation diffusion could be, in principle, studied by any physico-chemical process taking place in the oxide that is explicitly limited by the cation mobility. K. Salama et al.

recently reviewed several studies of creep involving perovskite-type oxides with respect to cation diffusion.[58] It was pointed out that creep processes are limited by cation diffusion since activation energies were higher than the activation energy for oxygen diffusion.[58] Nevertheless, it was not possible to determine from the creep studies alone which cation was rate-controlling.[58] It was pointed out that only a combination of at least two independent investigations can provide full information about deformation processes in these compounds.[58,59] Cation diffusion studies are needed also in order to fully understand a densification[60] or some solid state kinetic studies of perovskite materials.[61,62] These observations inevitably lead to a general conclusion that the systematic, experimental cation diffusion studies are necessary to fully understand many diffusion-limited processes in the perovskite-type oxides.

References

1. Bhalla, A. S.; Guo, R.; Roy, R. *Mat. Res. Innovat.* **2000**, *4*, 3.
2. Pena, M. A.; Fierro J. L. G. *Chem. Rev.* **2001**, *101*, 1981.
3. Tejuca, L. G.; Fierro, J. L. G.; Tascón, J. M. D. *Adv. Catal.* **1989**, *36*, 237.
4. Goldschmidt, V. M. Geochemisce Verterlungsgesetze der Elemente. Norske Videnskap, Oslo, 1927.
5. Glazer, A. M. *Acta Cryst. B* **1972**, *28*, 3384.
6. Glazer, A. M. *Acta Cryst. A* **1975**, *31*, 756.
7. Woodward, P. M. *Acta Cryst. B* **1997**, *53*, 44.
8. Van Roosmalen, J. A. M.; Corfunke, E. H. P.; Helmholdt, R. B.; Zandbergen, H. W. *J. Solid State Chem.* **1994**, *110*, 100.
9. Töpfer, J.; Goodenough, J. B. *J. Solid State Chem.* **1997**, *130*, 117.
10. Sakai, N.; Fjellvåg, H. *Acta Chem. Scand.* **1996**, *50*, 580.
11. Sakai, N.; Fellvåg, H.; Lebech, B. *Acta Chem. Scand.* **1997**, *51*, 904.
12. Thornton, G.; Tofield, B. C.; Hewat, A. W. *J. Solid State Chem.* **1986**, *61*, 301.
13. Kobayashi, Y.; Mitsunaga, T.; Fujinawa, G.; Arii, T.; Suetake, M.; Asai, K.; Harada, J. *J. Phys. Soc. Jpn.* **2000**, *69*, 3468.
14. Asai, K.; Yoneda, A.; Yokokura, O.; Tranquada, J. M.; Shirane, G.; Kohn, K. *J. Phys. Soc. Jpn.* **1998**, *67*, 290.
15. Radaelli, P. G.; Cheong, S.-W. *Phys. Rev. B* **2002**, *66*, 094408.
16. Geller, S.; Wood, E. A. *Acta Cryst.* **1956**, *9*, 563.
17. Fossdal, A.; Menon, M.; Wærnhus, I.; Wiik, K.; Einarsrud, M.-A.; Grande, T. *J. Am. Ceram. Soc.* **2004**, *87*, 1952.
18. Kharton, V. V.; Yaremchenko, A. A.; Naumovich, E. N. *J. Solid State Electrochem.* **1999**, *3*, 303.
19. Kuo, J. H.; Anderson, H. U.; Sparlin, D. M. *J. Solid State Chem.* **1989**, *83*, 52.
20. van Roosmalen, J. A. M.; van Vlaanderen, P.; Cordfunke, E. H. P.; Ijdo, W. L.; Ijdo, D. J. W. *J. Solid State Chem.* **1995**, *114*, 516.
21. Grundy, A. N.; Chen, M.; Hallstedt, B.; Gauckler, L. J. *J. Phase Equilib. Diffus.* **2005**, *26*, 131.
22. Mizusaki, J.; Mima, Y.; Yamauchi, S.; Fueki, K. *J. Solid State Chem.* **1989**, *80*, 102.

23. Bak, T.; Nowotny, J.; Rekas, M.; Ringer, S.; Sorrell, C. C. *Ionics* **2001**, *7*, 380.
24. Seppänen, M.; Kytö, M.; Taskinen, P. *Scand. J. Metall.* **1979**, *8*, 199.
25. Janecek, J. J.; Wirtz, G. P. *J. Am. Ceram. Soc.* **1978**, *61*, 242.
26. Petrov, A. N.; Cherepanov, V. A.; Zuev, A. Yu. *J. Solid State Electrochem.* **2006**, *10*, 517.
27. Mizusaki, J.; Sasamoto, T.; Cannon, W. R.; Bowen, H. K. *J. Am. Ceram. Soc.* **1982**, *65*, 363.
28. Wærnhus, I.; Vullum, P. E.; Holmestad, R.; Grande, T.; Wiik, K. *Solid State Ionics* **2005**, *176*, 2783.
29. Moruzzi, V. L.; Shafer, M. W. *J. Am. Ceram. Soc.* **1960**, *43*, 367.
30. Martin, M. in *Diffusion in condensed matter: methods, materials, models.* Heitjans, P.; Kärger, J.; Eds., Springer: Berlin, Germany, 2005, p 209.
31. Meher, H. *Mater. Trans. JIM* **1996**, *37*, 1259.
32. Islam, M. S. *J. Mater. Chem.* **2000**, *10*, 1027.
33. De Souza, R. A.; Islam, M. S.; Ivers-Tiffée, E. *J. Mater. Chem.* **1999**, *9*, 1621.
34. De Souza, R. A.; Maier, J. *J.Phys. Chem. Chem. Phys.* **2003**, *5*, 740.
35. Stølen, S.; Bakken, E.; Mohn, C. E. *Phys. Chem. Chem. Phys.* **2006**, *8*, 429.
36. Fisher, C. A. J.; Iwamoto, Y.; Asanuma, M.; Anyashiki, T.; Yabuta, K. *J. Eur. Ceram. Soc.* **2005**, *25*, 3243.
37. Kilo, M.; Taylor, M. A.; Argirusis, C.; Borchardt, G.; Jackson, R. A.; Schulz, O.; Martin, M.; Weller, M. *Solid State Ionics* **2004**, *175*, 823.
38. Schulz, O.; Martin, M.; Argirusis, C.; Borchardt, G. *Phys. Chem. Chem. Phys.* **2003**, *5*, 2308.
39. Freer, R. *J. Mater. Sci.* **1980**, *15*, 803.
40. Hong, J.-O.; Miyoshi, S.; Kaimai, A.; Nigara, Y.; Kawara, T.; Mizusaki, J. *Proc. - Electrochem. Soc.* **2001**, *2001-28*, 49.
41. Wærnhus, I.; Sakai, N.; Yokokawa, H.; Grande, T.; Einarsrud, M.-A.; Wiik, K. *Solid State Ionics* **2004**, *175*, 69.
42. Pavlyuchenko, M. M.; Filonov, B. O.; Shimanovich, I. E.; Prokudina, S. A. *Dokl. Akad. Nauk BSSR* **1970**, *14*, 328.
43. Petrov, A. N.; Rabinovich, L. Ya.; Zhukovskii, V. M.; Zhukovskaia, A. S. *Dokl. Chem.* **1987**, *292*, 18.
44. Matraszek, A.; Kobertz, D.; Singheiser, L.; Hilpert, K.; Kuncewicz-Kupczyk, W.; Miller, M.; Schulz, O.; Martin, M. *Mat.-wiss. u. Werkstofftech.* **2002**, *33*, 355.
45. Smith, J. B.; Norby, T.; Fossdal, A. *J. Am. Ceram. Soc.* **2006**, *89*, 582.
46. Akashi, T.; Nanko, M.; Maruyama, T.; Shiraishi, Y.; Tunabe, J. *J. Electrochem. Soc.* **1998**, *145*, 2090.
47. Akashi, T.; Mizuno, Y.; Nanko, M.; Maruyama, T.; Saiki, A.; Tsukui, K.; Tanabe, J. *Mater. Trans.* **2001**, *42*, 1411.
48. Kawamura, K.; Saiki, A.; Maruyama, T.; Nagata, K. *J. Electrochem. Soc.* **1995**, *142*, 3073.
49. Petrov, A. N.; Kropanev, A. Yu.; Zhukovskii, V. M.; Cherepanov, V. A.; Neudachina, G. K. *Russ. J. Inorg. Chem.* **1981**, *26*, 1708.
50. Smith, J. B.; Norby, T. *Solid State Ionics* **2006**, *177*, 639.

51. Sakai, N.; Horita, T.; Yamaji, K.; Brito, M. E.; Yokokawa, H.; Kawakami, A.; Matsuoka, S.; Watanabe, N.; Ueno, A. *J. Electrochem. Soc.* **2006**, *153*, A621.
52. Horita, T.; Ishikawa, M.; Yamaji, K.; Sakai, N.; Yokokawa, H.; Dokiya, M. *Solid State Ionics* **1999**, *124*, 301.
53. Horita, T.; Ishikawa, M.; Yamaji, K.; Sakai, N.; Yokokawa, H.; Dokiya, M. *Solid State Ionics* **1998**, *108*, 383.
54. Horita, T.; Sakai, N.; Kawada, T.; Yokokawa, H.; Dokiya, M. *J. Am. Ceram. Soc.* **1998**, *81*, 315.
55. Sakai, N.; Yamaji, K.; Horita, T.; Negishi, H.; Yokokawa, H. *Solid State Ionics* **2000**, *135*, 469.
56. Sakai, N.; Tsunoda, T.; Fukumoto, N.; Kojima, I.; Yamaji, K.; Horita, T.; Ishikawa, M.; Yokokawa, H.; Dokiya, M. *J. Electroceram.* **1999**, *4*, 121.
57. Vullum, P. E.; van Helvoort, A. T. J.; Holmestad, R.; Mastin, J.; Andersen, Ø. E.; Einarsrud, M.-A.; Grande, T. *J. Mater. Sci.* **2007**, in press.
58. Salama, K.; Majkic, G.; Balachandran, U. *Defect and Diffusion Forum* **2005**, *242-244*, 43.
59. Routbort, J. L.; Goretta, K. C.; Cook, R. E.; Wolfenstine, J. *Solid State Ionics* **2000**, *129*, 53.
60. Lin, M.-H.; Chou, J.-F.; Lu, H.-Y. *J. Eur. Ceram. Soc.* **2000**, *20*, 517.
61. Buscaglia, V.; Caracciolo, F.; Bottino, C.; Leoni, M.; Nanni, P. *Acta mater.* **1997**, *45*, 1213.
62. Buscaglia, V.; Buscaglia, M. T.; Giordano, L.; Martinelli, A.; Viviani, M.; Bottino, C. *Solid State Ionics* **2002**, *146*, 257.

4. Solid state diffusion

This section provides the necessary mathematical background for diffusion studies in solid state materials. The models and equations introduced in this section will be later actively used in the research papers of the thesis. The first chapter introduces the Fick's laws of diffusion. The solutions to the diffusion equation are mathematically derived for the diffusion from constant and instantaneous sources into a semi-infinite medium. The second chapter describes the chemical and tracer diffusion experiments. Analysis of both the inter-diffusion experiment and the reaction-diffusion experiment is provided. The last chapter deals with the mass transport in polycrystalline materials. The Fisher's model of grain boundary diffusion is described. Finally, the classification of diffusion kinetics in polycrystalline materials is discussed.

4.1. Fick's laws of diffusion

In a direct analogy with the heat flow, Fick expressed a mass flow of praticles due to a concentration gradient.[1] The mass flux, **J**, is proportional to the concentration gradient, i.e.,

$$\mathbf{J} = -\mathbf{D}\nabla\mathbf{c} \tag{4.1}$$

where c is the actual concentration of diffusing species, ∇ is a gradient vector operator, defined in the rectangular coordinate system as

$$\nabla = \mathbf{e}_x \frac{\partial}{\partial x} + \mathbf{e}_y \frac{\partial}{\partial y} + \mathbf{e}_z \frac{\partial}{\partial z} \tag{4.2}$$

and D is a proportionality constant called the diffusion coefficient. Equation (4.1) represents the Fick's first law of diffusion. Since the dimensions of **J** and ∇c in the SI system[2] are $m^{-2}s^{-1}$ and m^{-4} respectively, the dimension of the diffusion coefficient is m^2s^{-1}.

In practice, the solution of equation (4.1) requires the measurement of the steady-state concentration gradient and the steady-state flux. The steady-state conditions can not be often established during experiments due to, for example, time constraints. A materials balance in the volume element of the system then becomes useful.[3] This situation is illustrated in Fig. 1. The following expression in one dimension

$$\frac{\partial c}{\partial t} = -\frac{\partial J_x}{\partial x} \tag{4.3}$$

can be easily derived from Fig. 4.1. In three dimensions, equation (4.3) reads

$$\frac{\partial c}{\partial t} = - \nabla \mathbf{J} \tag{4.4}$$

Equation (4.4), upon substitution for **J** from equation (1), becomes

$$\frac{\partial c}{\partial t} = \nabla D(\nabla c) \tag{4.5}$$

If the diffusion coefficient is independent of coordinates, equation (4.5) becomes

$$\frac{\partial c}{\partial t} = D \Delta c \tag{4.6}$$

where Δ is a Laplacian operator, defined in the rectangular coordinate system as

$$\Delta = \nabla^2 = \frac{\partial^2}{\partial x^2} + \frac{\partial^2}{\partial y^2} + \frac{\partial^2}{\partial z^2} \tag{4.7}$$

Equation (4.6) is called the Fick's second law of diffusion, or, simply, the diffusion equation.

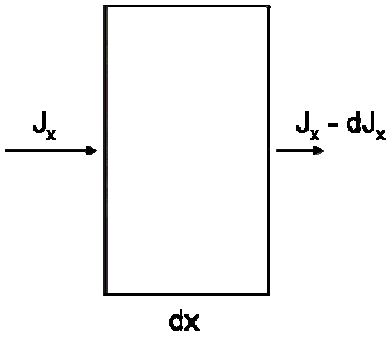

Fig. 4.1 One-dimensional mass balance in an infinitesimal system element.

4.2 Solutions to the diffusion equation

Experiments are usually designed in a way that the mass transport takes place mostly in one direction. The diffusion equation (4.6) then reduces to

$$\frac{\partial c}{\partial t} = D \frac{\partial^2 c}{\partial x^2} \tag{4.8}$$

The solutions of equation (4.8) are, for example, sought in the following form

$$c(x,t) \;=\; X(x)T(t) \tag{4.9}$$

where X(x) and T(t) are the functions of one variable only. Equation (4.9) forms the basis for the method of separation of variables.[1] Equation (4.8) can also be solved in the form of Laplace transforms. The Laplace transform of concentration $c(x,t)$ is, by definition, given as[3]

$$L\{c(x,t)\}_{t\to p} \;=\; \bar{c}(p) \;=\; \int_0^\infty \exp(-pt)c(x,t)\,dt \tag{4.10}$$

where $\bar{c}(p)$ is the image function, $\exp(-pt)$ is the Laplace kernel and p is a complex variable. If $c = c_0$ for all $t \geq 0$, it can be shown that

$$\bar{c}(p) \;=\; \int_0^\infty c_0 \exp(-pt)dt \;=\; \frac{c_0}{p} \tag{4.11}$$

Table 4.1 illustrates the most often used types of Laplace transforms.[3] In addition, the general theorems, taken from ref. 3, are given here

$$L\{c_1 + c_2\} \;=\; L\{c_1\} \;+\; L\{c_2\} \tag{4.12}$$

$$L\left\{\frac{\partial c}{\partial t}\right\} \;=\; pL\{c\} \;-\; c_0 \tag{4.13}$$

$$L\left\{\frac{\partial^n c}{\partial x^n}\right\} \;=\; \frac{\partial^n \bar{c}}{\partial x^n} \tag{4.14}$$

where c_0 is the initial concentration at t=0.

Table 4.1 Laplace transforms applicable to diffusion studies.

Laplace transform	Original function
$\bar{c}(p)$	$c(x,t)$
c_0 / p	c_0
$1/(p+\alpha)$	$\exp(-\alpha t)$
$\omega/(p^2+\omega^2)$	$\sin(\omega t)$
$p/(p^2+\omega^2)$	$\cos(\omega t)$
$\exp\{-(p/D)^{1/2} x\} \quad x>0$	$\frac{x}{2(\pi D t^3)^{1/2}} \exp\left(-\frac{x^2}{4Dt}\right)$
$\exp\{-(p/D)^{1/2} x\}/(p/D)^{1/2} \quad x>0$	$\left(\frac{D}{\pi t}\right)^{1/2} \exp\left(-\frac{x^2}{4Dt}\right)$
$\exp\{-(p/D)^{1/2} x\}/p \quad x>0$	$\operatorname{erfc}\left(\frac{x}{2\sqrt{Dt}}\right)$

4.2.1. Linear diffusion from a constant source into a semi-infinite medium

The diffusion equation (4.8) is a second order partial differential equation that requires two boundary or initial conditions in order to obtain a unique solution. In the case of linear diffusion from an infinite source into a semi-infinite medium, the initial condition is c=0 for x > 0 and t = 0. In addition, there is a boundary condition that requires c = c_0 at x = 0 for all t > 0.

By the use of equations (4.13) and (4.14), the diffusion equation can be transformed into[3]

$$\frac{\partial^2 \bar{c}}{\partial x^2} = \frac{p}{D}\bar{c} \tag{4.15}$$

Equation (4.15) is an ordinary differential equation. Its general solution is

$$\bar{c} = A\exp\left(-\sqrt{\frac{p}{D}}x\right) + B\exp\left(+\sqrt{\frac{p}{D}}x\right) \tag{4.16}$$

Only the first, decaying term satisfies the boundary condition and thus, B = 0. Parameter A is equal to c_0 / p since the Laplace transform of the initial condition is

$$\bar{c}(0) = \int_0^\infty c_0 \exp(-pt)\,dt = -\frac{c_0}{p}\exp(-pt)\Big|_0^\infty = \frac{c_0}{p} \tag{4.17}$$

The Laplace transform of the solution to the diffusion equation, therefore, becomes

$$\bar{c} = \frac{c_0}{p}\exp\left(-\sqrt{\frac{p}{D}}x\right) \tag{4.18}$$

Finally, referring to table 4.1, the solution to the diffusion equation becomes

$$c = c_0 \mathrm{erfc}\left(\frac{x}{2\sqrt{Dt}}\right) \tag{4.19}$$

where $\mathrm{erfc}\left(\frac{x}{2\sqrt{Dt}}\right)$ is a complementary error function of $\frac{x}{2\sqrt{Dt}}$. The complimentary error function is defined by the following equation

$$\mathrm{erfc}(z) = 1 - \mathrm{erf}(z) = 1 - \frac{2}{\sqrt{\pi}}\int_0^z \exp\left(-\eta^2\right)d\eta \tag{4.20}$$

4.2.2. Linear diffusion from an instantaneous source into an infinite medium

Another useful diffusion problem is a unidirectional diffusion from an instantaneous (finite) source into an infinite medium. This situation can be represented by a thin film source placed on a disk. The boundary condition requires that c = 0 for $x \rightarrow \infty$ and t > 0 s. In addition, the diffusion process is a subject to the mass constraint for a unit area given by the following equation[4]

$$\int_0^\infty c(x,t)\,dx = \frac{M}{2} \tag{4.21}$$

where M is a constant.

The Laplace transform of the solution to the diffusion equation is given by equation (4.16) with B = 0, i.e.

$$\bar{c} \;=\; A\exp\left(-\sqrt{\frac{p}{D}}x\right) \tag{4.22}$$

The Laplace transform of equation (4.21) yields

$$L\left\{\int_0^\infty c(x,t)\,dx\right\}_{t\to p} \;=\; L\left\{\frac{M}{2}\right\}_{t\to p} \tag{4.23}$$

The left-hand side of equation (4.23) is

$$\int_0^\infty \exp(-pt)\left\{\int_0^\infty c(x,t)\,dx\right\}dt \;=\; \int_0^\infty\left\{\int_0^\infty \exp(-pt)c(x,t)\,dt\right\}dx \;=\; \int_0^\infty \bar{c}\,(x,t)dx \tag{4.24}$$

Upon the substitution for $\bar{c}$ from equation (4.22) we obtain

$$L\left\{\int_0^\infty c(x,t)\,dx\right\}_{t\to p} \;=\; \int_0^\infty \bar{c}\,(x,t)dx \;=\; \int_0^\infty A\exp\left(-\sqrt{\frac{p}{D}}x\right)dx \;=\; \frac{A}{\sqrt{p/D}} \tag{4.25}$$

The right-hand side of equation (4.23) is equal to $\frac{M}{2p}$, see Table 1. This then, finally, yields

$$A \;=\; \frac{M}{2\sqrt{p/D}} \tag{4.26}$$

Eqaution (4.22) then becomes

$$\bar{c} \;=\; \frac{M}{2}\frac{1}{\sqrt{p/D}}\exp\left(-\sqrt{\frac{p}{D}}x\right) \tag{4.27}$$

The solution to the diffusion equation, upon the examination of Table 4.1, is

$$c \;=\; \frac{M}{2}\sqrt{\frac{D}{\pi t}}\exp\left(-\frac{x^2}{4Dt}\right) \tag{4.28}$$

The diffusion coefficient can be easily determined from the slope of the log c *vs*. x^2 plot.

4.3. Diffusion in materials

The diffusion in materials is characterized by several different diffusion coefficients since the diffusion experiment can be performed in several different ways. In the following, we shall distinguish between two different types of diffusion experiments.[5]

1. **Tracer diffusion experiment.** In this experiment, tiny amounts of the diffusing species are placed on the polished surface of the material (A) and annealed for a certain period of time. The total concentration of the trace element is usually very small and thus, the composition of the material is not affected by the presence of the tracer. Tracer diffusion experiments may be performed by the use of an isotope of the same element, A^*, or another element, B^*. We can therefore distinguish between the self-diffusion, D_{A*}, and impurity diffusion coefficients, D_{B*}. A factor that gives the ratio between the self- and impurity diffusion is called the segregation factor.

2. **Chemical diffusion experiment.** In this experiment, two different materials, A and B, are opposed and the diffusion between them occurs due to the concentration gradient. Two situations may happen depending on whether these two materials do react or not. If these materials do not react, an inter-diffusion between them usually occurs. If these materials do react, a third and, possibly, also fourth and fifth phases are formed at the interface between the reactants.

4.3.1 Concentration dependent diffusion

A first estimation of the inter-diffusion coefficient can be obtained from equation (4.19). Equation (4.19) can be rewritten in the following form

$$c = \frac{c^+ - c^-}{2}\operatorname{erfc}\left(\frac{x}{2\sqrt{Dt}}\right) + c^- \qquad (4.29)$$

where c^+ and c^- are the constants apparent from the experimental concentration profile. An illustration of the experimental penetration profile is given in Fig. 4.2.

If the diffusion coefficient is concentration-dependent, equation (4.29) does not suffice. The Boltzmann-Matano analysis should then be applied to evaluate the inter-diffusion coefficients from an experimental penetration profile.[5] The chemical diffusion coefficient, D, is, in general, concentration dependent. Equation (4.5), therefore, holds for the system. Equation (4.5) in one dimension is given by the following expression

$$\frac{\partial c}{\partial t} = \frac{\partial}{\partial x}\left(D\frac{\partial c}{\partial x}\right) \qquad (4.30)$$

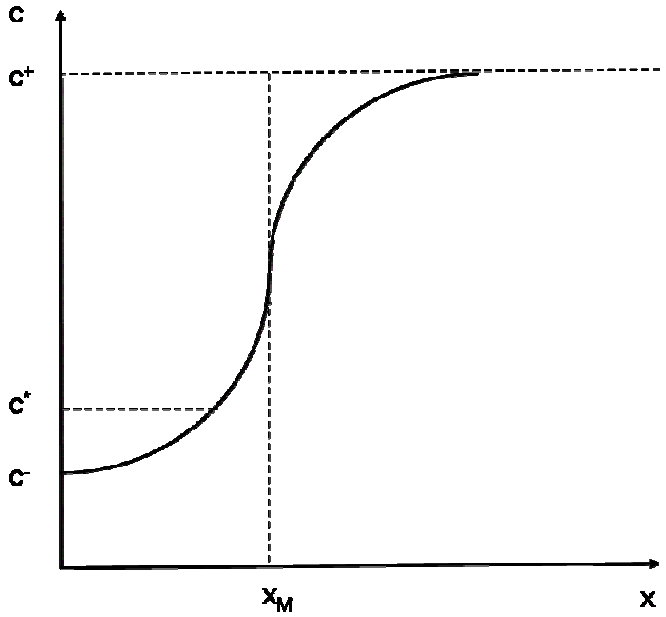

Fig. 4.2 Illustration of the inter-diffusion concentration profile.

It was shown by Boltzmann[1] that the partial differential equation (4.30) can be transformed to an ordinary differential equation by the introduction of a new variable, η, given by the following definition[1]

$$\eta = \frac{x}{2\sqrt{t}} \tag{4.31}$$

The following transformations are then valid

$$\frac{\partial c}{\partial x} = \frac{1}{2\sqrt{t}}\frac{dc}{d\eta} \tag{4.32}$$

$$\frac{\partial}{\partial x}\left(D\frac{\partial c}{\partial x}\right) = \frac{1}{4t}\frac{d}{d\eta}\left(D\frac{dc}{d\eta}\right) \tag{4.33}$$

$$\frac{\partial c}{\partial t} = -\frac{x}{4t^{\frac{3}{2}}}\frac{dc}{d\eta} \tag{4.34}$$

Equation (4.30) then finally becomes

$$-2\eta\frac{dc}{d\eta} = \frac{d}{d\eta}\left(D\frac{dc}{d\eta}\right) \tag{4.35}$$

Equation (4.35) can be integrated with respect to η as follows

$$-2\int_{c^-}^{c^*}\eta dc = \left[D\frac{dc}{d\eta}\right]_{c^-}^{c^*} = D(c^*)\left(\frac{dc}{d\eta}\right)_{c=c^*} \tag{4.36}$$

since $D\,dc/d\eta = 0$ when $c=c^-$ (Fig. 4.2). The rearrangement of equation (4.36) provides the following expression

$$D(c^*) = -\frac{2}{\left(\frac{dc}{d\eta}\right)_{c=c^*}}\int_{c^-}^{c^*}\eta dc \tag{4.37}$$

Upon the substitution for η from equation (4.31), equation (4.37) finally becomes

$$D(c^*) = -\frac{1}{2t\left(\frac{dc}{dx}\right)_{c=c^*}}\int_{c^-}^{c^*}x dc \tag{4.38}$$

Since also $D\,dc/d\eta = 0$ when $c=c^+$, it follows from equation (4.36) that x must satisfy the following condition

$$\int_{c^-}^{c^+}\eta dc = \int_{c^-}^{c^+}x dc = 0 \tag{4.39}$$

The distance x must therefore be measured from the position x_M given in Fig. 4.2. This plane is called the Matano plane.[1]

The accurate location of the Matano plane is often complicated, especially in the non-symmetric concentration profiles. den Broeder therefore provided an alternative approach that avoids the location of the Matano interface.[6] By the use of the following variable

$$y_c = \frac{c-c^-}{c^+-c^-} \tag{4.40}$$

equation (4.38) can be rewritten in the following way

$$D(c^*) = -\frac{1}{2t\left(\frac{dc}{dx}\right)_{x=x^*}}\left\{(1-y_{c^*})\int_{-\infty}^{x^*}(c-c^-)\,dx + y_{c^*}\int_{x^*}^{\infty}(c^+-c)\,dx\right\} \quad (4.41)$$

Equations (4.39) and (4.41) are equivalent in terms of the accuracy of the result. This was recently confirmed by Kailasam et al.[7]

The intrinsic chemical diffusion coefficients of pure components A and B, D_A and D_B, can finally be obtained by the extrapolation of the concentration-dependent diffusion coefficient at $c_A \to \infty$ (or $c_B \to 0$) and $c_B \to \infty$ (or $c_A \to 0$) respectively.

4.3.2 Kirkendall effect

In general, chemical diffusion experiments of two different components, D_A and D_B, differ. Due to this reason, the original interface (Kirkendall plane) between the materials moves during the experiment.[5] This situation is schematically given in Fig. 4.3. It is, therefore, necessary to place inert markers between two materials in order to track the position of the initial interface. The movement of the marker, v_K, is a function of the individual chemical diffusion coefficients and it is given by the Kirkendall equation

$$v_K = (D_A - D_B)\frac{\partial X_A}{\partial x} \quad (4.42)$$

where $\frac{\partial X_A}{\partial x}$ is the concentration gradient at the Kirkendall plane.

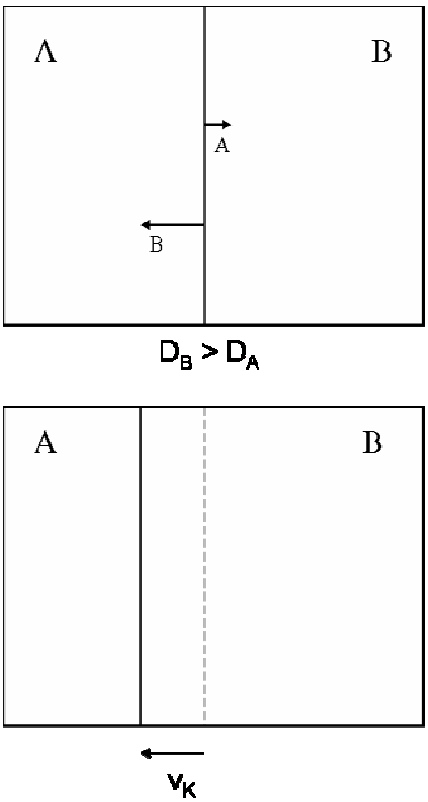

Fig. 4.3 Illustration of the Kirkendall effect in an inter-diffusion couple composed of two pure metal A and B.

4.3.3. Formation of a chemical compound layer at the interface of two elementary substances

V. I. Dybkov[8] recently reviewed the experimental data on solid state reaction kinetics between two metal components, A and B.

$$pA + qB \rightarrow A_pB_q \qquad (4.43)$$

The conclusions from the study are the following[8]:

1. The solid-state growth of the layer of any chemical compound A_pB_q between two mutually insoluble elementary substances A and B is due to two parallel partial processes:
   a) diffusion of atoms of a given component across the bulk of the layer,
   b) chemical transformations with the participation of these atoms and the surface atoms of another component (interface reactions).
2. Both interface reactions as well as diffusion fluxes of the components across the bulk of a growing compound layer are independent of each other.

3. The layer thickness-time dependence is, in general, described by a linear to parabolic equation. Its initial region is close to a straight line. This region then transforms gradually to a parabola. The higher the temperature the narrower is the region of linear growth.
4. There are two critical values of the layer thickness, $x_{1/2}^{A}$ and $x_{1/2}^{B}$, that divide the layer thickness-time dependence into the reaction-controlled and diffusion-controlled regions with respect to the components A and B respectively.
5. For any chemical compound A_pB_q, the reaction-diffusion and self-diffusion coefficients of a given component (A or B) are, in general, different, the former being much greater than the latter. Nevertheless, after normalising to the same vacancy concentration, these become close, if not identical, provided that the mechanism of diffusion is of a vacancy type in both the growing and non-growing layer of that compound.
6. The different contributions of the components to the growth process of the layer at the interface between phases A and B should not be regarded as a result of the Kirkendall's effect. The Kirkendall's effect reflects the different diffusivities of A and B in a solid solution of A in B or B in A respectively. It does not reflect the different diffusivities of A or B in an intermetallic compound A_pB_q which has, in general, a very narrow solid solubility range.

The relationship between the experimentally observed parabolic rate constant and the chemical diffusion coefficient of diffusing species in the bulk of the layer is not simple. The parabolic rate constant is, in fact, a function of both component diffusivities, D_A and D_B, and a function of the standard Gibb's energy of the solid state reaction. Schmalzried provided the following equation for the parabolic rate constant of reaction (4.43)[9]

$$k = \left(\frac{D_A}{p} + \frac{D_B}{q}\right)\frac{\Delta G^0_{A_pB_q}}{RT} \tag{4.44}$$

where $\Delta G^0_{A_pB_q}$ is the standard Gibb's energy of reaction (4.43) and k is a parabolic rate constant. The parabolic rate law is generally expressed as

$$x^2 = 2kt + C \tag{4.45}$$

where C is an integration constant. Equation (4.45) comes from the integration of the following kinetic equation, observed experimentally

$$v = \frac{dx}{dt} = kx^{-1} \tag{4.46}$$

where v is the rate of the reaction (4.43).

The analysis of the solid state reaction kinetics between oxides is a very complex process since the number of possible mobile components and, correspondingly, the number of possible reaction mechanisms, increase dramatically. Only a few reactions have been studied both theoretically and experimentally.[9] Further mathematical treatment of reactive diffusion couples will be provided in papers I and II.

4.3.4 Grain boundary diffusion

4.3.4.1 Fisher's diffusion model along single grain boundary

The diffusion in solids is known to occur along grain boundaries (GB) and over free surfaces more rapidly than through interiors of crystals. Most mathematical treatments are based on the Fisher's model describing diffusion along a single GB.[10,11,12] This model is also called an isolated boundary model. The GB is represented by a semi-infinite slab embedded in an isotropic crystal perpendicular to its surface. The schematic representation is given in Fig. 4.4. The GB is described by two physical parameters: the GB width δ and the GB diffusion coefficient D_{GB}.

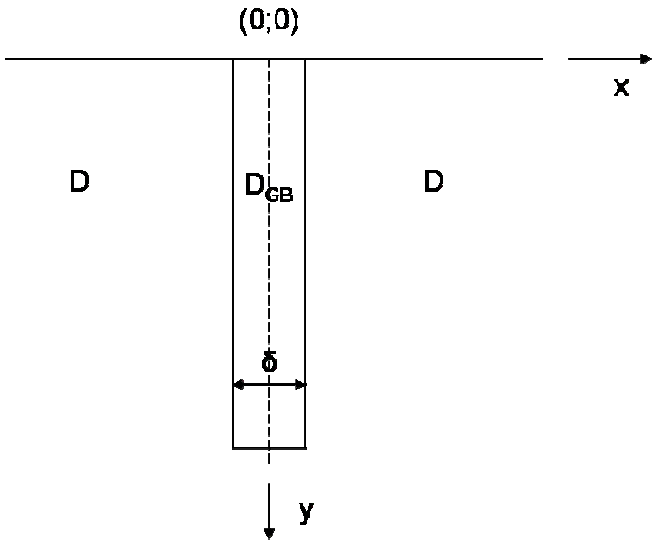

Fig. 4.4 The Fisher's model of the grain boundary.

A derivation of the diffusion equation for this system is based on the following assumptions:[11]

1. The Fick's laws of diffusion are obeyed in both the crystal and the grain boundary slab.
2. The diffusion coefficients in the bulk and in the grain boundary slab are isotropic and independent of the concentration, position and time.

3. The diffusant flow is continuous at the grain boundary/crystal interface. This necessarily means that the diffusant concentration and the flux are continuous at $x = \pm\delta/2$.
4. The width of the grain boundary is small and therefore, the concentration variation across it in the x-direction is negligible.

The diffusion process is then described by the following two second-order partial differential equations[11]

$$\frac{\partial c}{\partial t} = D\left(\frac{\partial^2 c}{\partial x^2} + \frac{\partial^2 c}{\partial y^2}\right) \qquad \text{for } |x| > \delta/2 \tag{4.47}$$

$$\frac{\partial c_{GB}}{\partial t} = D_{GB}\frac{\partial^2 c_{GB}}{\partial x^2} + \frac{2D}{\delta}\left(\frac{\partial c}{\partial x}\right)_{x=\delta/2} \tag{4.48}$$

where c, c_{GB}, D and D_{GB} are the concentrations and diffusion coefficients in the bulk and along grain boundaries respectively. The solutions to equations (4.47) and (4.48) must meet the initial and boundary conditions. In addition, a condition of continuity between bulk and grain boundary concentration must be met, i.e.

$$c_{GB}(y,t) = c(\pm\delta/2, y, t) \tag{4.49}$$

as well as a surface condition. The surface condition for the diffusion from a constant source is

$$c(x,0,t) = c_0 = \text{const.} \tag{4.50}$$

The surface condition for the diffusion from a thin-film source can be given as

$$c(x,y,0) = M\delta(y), \qquad c(x,0,t) = \frac{M}{\sqrt{\pi Dt}} \tag{4.51}$$

where M is a constant.

Fisher postulated that the bulk diffusion occurs due to the leakage of diffusing species from the grain boundary. The bulk diffusion can be, therefore, given approximately as[11]

$$c(x,y,t) \approx c_{GB}(y,t)\,\text{erfc}\left(\frac{x}{2\sqrt{Dt}}\right) \tag{4.52}$$

The average concentration found at the distance y from the surface, $\langle c \rangle$, then obeys the following proportionality

$$\langle c \rangle \sim c_0 \exp\left(-\pi^{-1/4} w\right) \tag{4.53}$$

with

$$w = \frac{y}{\sqrt{\delta D_{GB}}}\left(\frac{4D}{t}\right)^{1/4} \tag{4.54}$$

This equation means that the plot of $\log\langle c \rangle$ *vs.* y should yield a straight line. The product δD_{GB} can be, then, calculated by the following equation

$$\delta D_{GB} = 1.128\sqrt{\frac{D}{t}}\left(-\frac{\partial \ln\langle c \rangle}{\partial y}\right)^{-2} \tag{4.55}$$

where $\frac{\partial \ln\langle c \rangle}{\partial y}$ is a slope of the experimental $\ln\langle c \rangle vs. y$ plot. Whipple later refined Fisher's solution[11] and found that for the diffusion from constant and instantaneous sources it is possible to write

$$\frac{\partial \ln\langle c \rangle}{\partial w^{6/5}} = -0.78 \tag{4.56}$$

The power of 6/5 has no physical meaning; it only provides a good numerical approximation of the exact profile. Equation (4.55) than transforms into the following, widely used form

$$\delta D_{GB} = 1.32\sqrt{\frac{D}{t}}\left(-\frac{\partial \ln\langle c \rangle}{\partial y^{6/5}}\right)^{-5/3} = 0.33\sqrt{\frac{D}{t}}\left(-\frac{\partial \log\langle c \rangle}{\partial y^{6/5}}\right)^{-5/3} \tag{4.57}$$

The validity of equations (4.56) and (4.57) requires the parameter α, given as

$$\alpha = \frac{\delta}{2\sqrt{Dt}} \tag{4.58}$$

to be $\alpha < 0.1$ and β, given as

$$\beta = \frac{\delta D_{GB}}{2D\sqrt{Dt}} \tag{4.59}$$

to be $\beta > 10$. Equation (4.57) thus can only be applied to the long penetration "tail" caused by the simultaneous GB and bulk diffusion. A near-surface region, caused by the direct volume diffusion from the surface, can not be used to obtain GB diffusion data.

4.3.4.2 Harrison's classification of diffusion kinetics

The GB diffusion is a complex process involving several elementary steps. These steps include the direct volume diffusion from the surface, the diffusion along GBs, the partial leakage of the diffusant from the GBs to the grains and the subsequent volume diffusion around the GBs. In each particular regime one or two elementary processes control the overall rate of diffusion. Each regime dominates in a certain region of annealing temperatures, grain sizes and other experimental parameters. In the following, we shall present the Harrison's classification of diffusion kinetics.[11,12] It is schematically given in Fig. 4.5. It is the most widely used classification of diffusion kinetics in polycrystal.

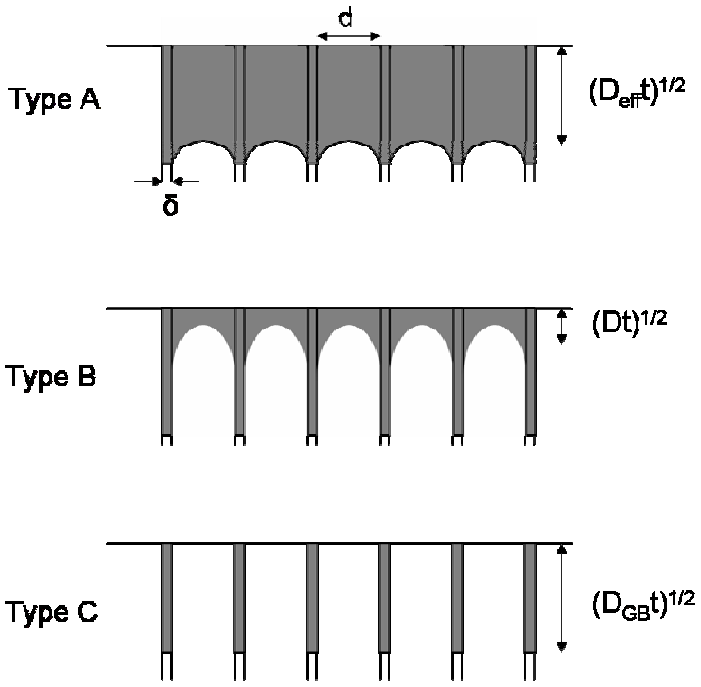

Fig. 4.5 Harrison's classification of diffusion kinetics in polycrystal

In the A type of diffusion kinetics, the volume diffusion length is larger than the spacing between grain boundaries. The condition of the A regime is

$$\sqrt{Dt} \gg d \tag{4.60}$$

On the macroscopic scale, the diffusion in a polycrystal obeys the Fick's law with an effective diffusion coefficient D_{eff}. The effective diffusion coefficient is given by the following equation

$$D_{\text{eff}} = fD_{\text{GB}} + (1-f)D \tag{4.61}$$

where D and D_{GB} are the bulk and grain boundary diffusion coefficients respectively and f is the volume fraction of the grain boundaries in the polycrystal. Equation (4.61) represents the Hart's formula.[9] The volume fraction of grain boundaries depends on the grain size. The bulk and grain boundary diffusion coefficients can, therefore, be determined from equation (4.61) if the diffusion experiment is performed on materials with different grain sizes.

In the B regime, the volume diffusion length is shorter than the spacing between the grain boundaries. This can be written as

$$\delta \ll \sqrt{Dt} \ll d \tag{4.62}$$

In this case, the volume diffusion from the neighbouring GBs does not overlap and the individual GBs are effectively isolated. In this regime, the penetration profile has a two-step shape. A near-surface region is caused by the direct diffusion from the surface and therefore, this region can be used to evaluate the bulk diffusion coefficient using equations (4.19) or (4.28). A long penetration tail is caused by a simultaneous bulk and GB diffusion. GB diffusivity can, therefore, be obtained from equation (4.57).

In the type C kinetics, observed at low temperatures, the volume diffusion is "frozen out". It can be written that

$$\sqrt{Dt} \ll \delta \tag{4.63}$$

In this case, the diffusant penetrated into the sample is located only at the grain boundaries. This regime can be, therefore, used to obtain the GB diffusion coefficient directly. The GB width does not need to be necessarily known. Nevertheless, the analysis of the experimental penetration profile may be extremely difficult since the amount of penetrated species is usually very small.

Beside the Harrison's model of parallel GBs, also other models have been proposed. These include the cubic grain model of Suzuoka, the spherical grain model of Bokshtein et al. and the general model of diffusion in isotropic polycrystals by Levine and MacCallum.[12] Nevertheless; it has to be kept in mind that the shape and the grain size of most polycrystalline materials are not uniform. The Harrison's model of parallel GBs remains one of the most useful models of the diffusion kinetics in polycrystals.

References

1. Crank, J. *Mathematics of diffusion*, Oxford University Press, Great Britain, 1956.
2. Aylward, G. H.; Findlay, T. J. V. *SI Chemical data*; John Wiley & Sons: Sydney, Australia, 1971.
3. Kirkaldy, J. S.; Young, D. J. *Diffusion in the condensed state*, The Institute of Metals: London, Great Britain, 1987.
4. Glicksman, M. E.; Lupulescu, A. *Module 3:; Solutions to the linear diffusion equation*, http://www.rpi.edu/locker/40/001240/diff_mods/Diff03.ppt
5. Mehrer, H. in *Diffusion in Condensed Matter: Methods, Materials, Models;* Heitjans, P.; Kärger J., Eds.; Springer: Berlin, Germany, 2005, p 3.
6. den Broeder, F. J. A. *Scripta Metallurgica* **1969**, *3*, 321.
7. Kailasam, S. K.; Lacombe, J. C.; Glicksman, M. E. *Metall. Mater. Trans. A* **1999**, *30*, 2605.
8. Dybkov, V. I., *Reaction diffusion and solid state reaction kinetics,* The IPMS Publications, Kyiv, Ukraine, 2002.
9. Schmalzried, H. *Chemical Kinetics of Solids*, VCH Verlagsgesellschaft mbH, Weinheim, Germany, 1995.
10. Fisher, J. C. *J. Appl. Phys.* **1951**, *22*, 74.
11. Kaur, I.; Mishin, Y.; Gust, W. *Fundamentals of Grain and Interphase Boundary Diffusion,* John Wiley & Sons Ltd.: Chichester, Great Britain, 1995.
12. Herzig, C.; Mishin, Y. in *Diffusion in Condensed Matter: Methods, Materials, Models;* Heitjans, P.; Kärger J., Eds.; Springer: Berlin, Germany, 2005, p 337.

Paper I

Cation self-diffusion and nonstoichiometry of lanthanum manganite studied by diffusion couple measurements*

Marián Palcut, Kjell Wiik and Tor Grande

Department of Materials Science and Engineering, Norwegian University of Science and Technology, 7491 Trondheim, Norway

Abstract

Reaction kinetics between dense, polycrystalline pellets of La_2O_3 and Mn_3O_4 were investigated at temperatures 1370-1673 K and oxygen partial pressures 40 Pa - 50 kPa. The formation of single product phase, nonstoichiometric $La_{1-x}Mn_{1-y}O_{3\pm\delta}$, was confirmed by X-ray diffraction and electron microprobe analysis. The solid solubility limits of $La_{1-x}Mn_{1-y}O_{3\pm\delta}$ determined by wave dispersive spectroscopy were in good agreement with previous reports and equilibrium was achieved at the phase boundaries in the diffusion couples. Vacancies at the La and O sub-lattices are proposed to be the dominating point defects in the product layer. The growth of the product phase followed the parabolic rate law regardless of temperature and oxygen partial pressure. Location of Pt-markers demonstrated that diffusion of Mn cations in $La_{1-x}Mn_{1-y}O_{3\pm\delta}$ dominated over diffusion of La^{3+}. The diffusion coefficient of Mn^{3+} was determined from the parabolic rate constant and activation energy of (280±40) kJ mol^{-1} was found. Results are discussed in relation to cation diffusion in other $LaBO_{3\pm\delta}$ oxides (B = Cr^{3+}, Mn^{3+}, Fe^{3+}).

Keywords: $LaMnO_3$, solid solution, diffusion-controlled solid state reaction kinetics, cation transport, perovskite

http://dx.doi.org/10.1021/jp0642746

*****published in *J. Phys. Chem. C* **2007**, *111*, 813.

Paper II

Cation self-diffusion in $LaCoO_3$ and La_2CoO_4 studied by diffusion couple experiments*

Marián Palcut, Kjell Wiik and Tor Grande

Department of Materials Science and Engineering, Norwegian University of Science and Technology, 7491 Trondheim, Norway

Abstract

Reaction kinetics between dense, polycrystalline pellets of La_2O_3 and CoO were investigated at temperatures 1370-1673 K and oxygen partial pressures 40 Pa - 50 kPa. At high oxygen partial pressures, single phase $LaCoO_3$ was formed. The growth of the $LaCoO_3$ phase followed the parabolic rate law. Location of Pt-markers demonstrated that diffusion of Co cations in $LaCoO_3$ dominated over diffusion of La^{3+}. The diffusion coefficient of Co^{3+} was determined from the parabolic rate constant and activation energy of (250±10) kJ mol^{-1} was found. Diffusion coefficient of Co^{3+} in $LaCoO_3$ decreased with decreasing oxygen partial pressure. At the lowest oxygen partial pressure investigated, two product phases, $LaCoO_3$ and La_2CoO_4, were observed. Diffusion coefficient of Co cations in La_2CoO_4 was estimated. Results were discussed in relation to cation diffusion in other $LnBO_3$ oxides (B = Cr^{3+}, Mn^{3+}, Fe^{3+}). A correlation between diffusion of the B-cation and the melting point was found for $LnBO_3$ materials.

Keywords: La-Co-O system, diffusion-controlled solid state reaction kinetics, cation transport, perovskite

http://dx.doi.org/10.1021/jp068343s

*published in *J. Phys. Chem. B* **2007**, *111*, 2299.

Paper III

Tracer diffusion of ^{141}Pr in $LaMnO_3$, $LaCoO_3$ and $LaFeO_3$ materials*

Marián Palcut,[a] Jens S. Christensen,[b] Kjell Wiik[a] and Tor Grande[a]

[a]Department of Materials Science and Engineering, Norwegian University of Science and Technology, 7491 Trondheim, Norway

[b]Department of Physics, University of Oslo, 0316 Oslo, Norway

Abstract

Impurity diffusion of Pr^{3+} in dense polycrystalline $LaMnO_3$, $LaCoO_3$ and $LaFeO_3$ respectively was studied at 1373 – 1673 K in air in order to shed a light on La-site vacancy migration in these materials. Cation distribution profiles was studied by secondary ion mass spectrometry and it was found that penetration profiles of Pr^{3+} had two distinct regions with different slopes. First, shallow region was used to evaluate bulk diffusion coefficients. The activation energies for bulk diffusion of Pr^{3+} in $LaMnO_3$, $LaCoO_3$ and $LaFeO_3$ were (47 ± 31), (141 ± 40) and (198 ± 84) kJ mol^{-1} respectively, which are significantly lower than previously predicted by atomistic simulations. Bulk diffusion of Pr^{3+} in $LaMnO_3$ was enhanced compared to $LaCoO_3$ and $LaFeO_3$ due to higher concentrations of intrinsic point defects in $LaMnO_3$, especially La-site vacancies. Grain boundary diffusion coefficients of Pr^{3+} in $LaCoO_3$ and $LaFeO_3$ materials were evaluated according to Whipple-Le Claire's equation. Activation energies for grain boundary diffusion of Pr^{3+} in $LaCoO_3$ and $LaFeO_3$ materials respectively were (173 ± 24) and (196 ± 74) kJ mol^{-1}. Finally, a correlation between activation energies for cation diffusion in bulk and along grain boundaries in pure and substituted $LaBO_3$ materials (B = Cr, Fe, Co) was found and discussed.

*submitted to *J. Phys. Chem.* (7th May 2007)

Paper IV

Cation inter-diffusion between $LaMnO_3$ and $LaCoO_3$ materials*

Marián Palcut, Kjell Wiik and Tor Grande

Department of Materials Science and Engineering, Norwegian University of Science and Technology, NO-7491 Trondheim, Norway

Abstract

Cation inter-diffusion between $LaMnO_3$ and $LaCoO_3$ materials was investigated at 1383 – 1683 K in air by electron microprobe analysis. The penetration of Co^{3+} into $LaMnO_3$ was observed to be significantly more pronounced than the Mn^{3+} diffusion in $LaCoO_3$. The inter-diffusion of Co^{3+} into $LaMnO_3$ resulted in the formation of solid solution $LaMn_{1-x}Co_xO_3$(ss) in line with the previous phase diagram studies. The bulk diffusion coefficients of Co^{3+} in $LaMn_{1-x}Co_xO_3$(ss) were evaluated and an activation energy of (197 ± 17) kJ mol^{-1} was found. Element mapping of the cross section of $LaCoO_3$ revealed a preferential grain boundary diffusion of Mn^{3+} in $LaCoO_3$. The low bulk diffusion of Mn^{3+} in $LaCoO_3$ relative to the bulk diffusion of Co^{3+} in $LaMnO_3$ reflects the lower cation vacancy concentration in the later material. The difference in activation energy for the impurity diffusion of Co^{3+} in $LaMnO_3$ and self-diffusion of Mn^{3+} in $LaMnO_3$ reported previously, was discussed with respect to the contributions of vacancy formation and migration enthalpies reflecting the different thermal history of the materials. The estimated energies for the partial Schottky equilibrium of $LaMnO_3$ and $LaCoO_3$ materials were significantly lower than previously estimated by atomistic simulations.

*submitted to *J. Phys. Chem. Solids* (16th June 2007)

Appendix

Cation Self-Diffusion and Non stoichiometry of Lanthanum Manganite Studied by Diffusion Couple Measurements

Marian Palcut, Kjell Wiik, and Tor Grande* Department of Materials Science and Engineering, Norwegian University of Science and Technology, 7491 Trondheim, Norway

J. Phys. Chem.C 2007, 111, 813-822
http://dx.doi.org/10.1021/jp0642746